DISSERTATIONES
TECHNOLOGIAE
UNIVERSITATIS
TARTUENSIS
97

HANS PRIKS

Life within 3D-printed engineered living materials based on micellar hydrogels

DISSERTATIONES TECHNOLOGIAE UNIVERSITATIS TARTUENSIS
97

DISSERTATIONES TECHNOLOGIAE UNIVERSITATIS TARTUENSIS
97

HANS PRIKS

Life within 3D-printed engineered living materials based on micellar hydrogels

UNIVERSITY OF TARTU
Press
1632

The doctoral studies were carried out at the Institute of Technology, Faculty of Science and Technology, University of Tartu, Estonia.

This dissertation was accepted for the commencement of the degree of Doctor of Philosophy in Environmental Technology on 23.12.2025 by the Joint Council of the Doctoral Programme of Engineering and Technology at the University of Tartu.

Supervisor: Tarmo Tamm, PhD
Professor of Materials Engineering
Institute of Technology, University of Tartu, Estonia

Reviewer: Karin Kogermann, PhD
Professor in Physical Pharmacy
Institute of Pharmacy, University of Tartu, Estonia

Opponent: Johan Ulrik Lind, PhD
Associate Professor at the Department of Health Technology
Technical University of Denmark, Denmark

Commencement: January 29th 2026, at 14.15, Auditorium 121, Nooruse 1, Tartu.

Publication of this thesis is granted by the Institute of Technology, Faculty of Science and Technology, University of Tartu.

ISSN 2228-0855 (print)
ISBN 978-9908-57-104-1 (print)
ISSN 2806-2620 (pdf)
ISBN 978-9908-57-105-8 (pdf)

University of Tartu Press
www.tyk.ee

TABLE OF CONTENTS

LIST OF ORIGINAL PUBLICATIONS

The present thesis is based on the following original publications, which are referred to in the text by their corresponding Roman numerals:

I. **Priks, H.**, Butelmann, T., Illarionov, A., Johnston, T. G., Fellin, C., Tamm, T., Nelson, A., Kumar, R., & Lahtvee, P.-J. (2020). Physical Confinement Impacts Cellular Phenotypes within Living Materials. *ACS Applied Bio Materials*, 3(7), 4273–4281. https://doi.org/10.1021/acsabm.0c00335

II. Johnston, T. G., Fillman, J. P., **Priks, H.**, Butelmann, T., Tamm, T., Kumar, R., Lahtvee, P. J., & Nelson, A. (2020). Cell-Laden Hydrogels for Multikingdom 3D Printing. *Macromolecular Bioscience*, *2000121*, 1–7. https://doi.org/10.1002/mabi.202000121

III. Butelmann, T., **Priks, H.**, Parent, Z., Johnston, T. G., Tamm, T., Nelson, A., Lahtvee, P. J., & Kumar, R. (2021). Metabolism Control in 3D-Printed Living Materials Improves Fermentation. *ACS Applied Bio Materials*, *4*(9), 7195–7203. https://doi.org/10.1021/acsabm.1c00754

IV. **Priks, H.**, Zadin, V., Talgre, I. R., Zekker, I., & Tamm, T. (2025). Linking physical properties of micellar hydrogels to engineered living material performance. *Materials and Design*, *256*. https://doi.org/10.1016/j.matdes.2025.114347

Related methodological publication:
Priks, H., & Butelmann, T. (2020). *Scanning electron microscopy (SEM) protocol for imaging living materials v1*. https://doi.org/10.17504/protocols.io.bekcjcsw

Author's contribution

I. The author contributed to the study design, constructed the 3D printing setup, prepared the samples, developed the SEM protocol for sample preparation and imaging, participated in data acquisition and analysis, and took part in the writing and editing of the manuscript.

II. The author assisted in setting up dual-extrusion 3D printing, prepared SEM samples for imaging, and contributed to the writing of the manuscript.

III. The author supervised the first author in hydrogel handling and sample preparation, contributed to conceptual ideas, and provided comments on the manuscript.

IV. The author initiated the study, designed and constructed the experimental apparatus, performed the majority of the experiments and data analysis, and wrote the manuscript.

ABBREVIATIONS

3D	three-dimensional
BUM	bisurethane methacrylate
CAD	computer-aided design
DMA	dimethacrylate
ELM	engineered living material
EtOH	ethanol
HLM	hybrid living material
LAB	laser-assisted bioprinting
OM	optical microscopy
PBS	phosphate-buffered saline
PEO	polyethylene oxide
PGE	poly(isopropyl glycidyl ether-stat-ethyl glycidyl ether) — polyethylene oxide — poly(isopropyl glycidyl ether-stat-ethyl glycidyl ether)
PPO	polypropylene oxide
SC	suspension culture
SEM	scanning electron microscopy
SLA	stereolithography
UV	ultraviolet

TERMINOLOGY AND TECHNICAL SPECIFICATIONS

In this dissertation:

- **'Construct'** refers to the overall three-dimensional (3D) object at the millimetre–centimetre scale. It is used as a term for the final, macroscale geometry.
- **'Structure'** refers to the internal architecture at the intermediate (mesoscale) level, such as printed layers, channels, or compartmental patterns (typically tens to hundreds of micrometres to millimetres). The term emphasises how the construct is organised into distinct domains or features.
- **'Matrix'** refers to the polymer phase at the micro- and nanoscale, such as the crosslinked hydrogel network that directly surrounds and embeds the cells (typically nanometre to micrometre length scales).
    - The plural form 'matrices' is used when comparing different polymer formulations (e.g. "F127-BUM and PGE-DMA matrices").
    - In cell-laden systems, 'matrix' emphasises the local microenvironment experienced by the cells, whereas 'construct' emphasises the macroscopic printed object.

1. INTRODUCTION

For decades, our global economy has followed a linear economy model — "take-make-waste". This approach has been highly efficient in the short term but has had devastating effects on the environment in the long run. Fossil fuels have powered our industries, plastics have shaped our world, and the culture of consumption has led to mountains of waste. However, this progress has come at a cost: rising temperatures, erratic weather patterns, and degraded ecosystems that sustain life. For many, the answer lies in the concept of a circular bioeconomy, where biological resources replace fossil fuels as the backbone of industry and resources are kept in circulation as long as possible.

At the heart of this transition lies biotechnology. Living cells, such as bacteria, yeast, algae, and mammalian cells, can act as miniature factories that convert renewable feedstocks into valuable products. Advances in genetic engineering and synthetic biology have enabled these systems to be programmed with increasing precision for industrial and environmental purposes, broadening the range of products and functions achievable through biological means.

However, these cells also have limitations. They typically require carefully controlled and sterile environments to maintain productivity. Over time, especially in complex or changing environments, their performance can deteriorate due to genetic instability and the accumulation of mutations, leading to the loss of function or uncontrolled proliferation. Furthermore, ensuring biocontainment and preventing genetic leakage into natural ecosystems remain persistent challenges. These limitations underscore the need for material-based strategies — such as encapsulating cells to create engineered living materials (ELMs) — that provide physical control, environmental buffering, and stable microenvironments to enhance the robustness of these synthetic biological systems. In this field, many bio-based and biopolymer materials have been explored. However, most of these are not biologically inert and can therefore be susceptible to microbial degradation or enzymatic breakdown by the very organisms they are intended to host, limiting their use in longer-term biomanufacturing scenarios.

This thesis investigates synthetic, photo-crosslinkable micellar hydrogels as structural platforms for three-dimensional (3D) printing of ELMs. It examines how triblock copolymer micellar architecture and mechanical characteristics influence the behaviour of encapsulated microorganisms. Through combined experimental characterisation, microscopy, and in silico modelling, the work reveals the interplay between polymer mechanics and microbial physiology, showing how confinement and polymer–cell interactions shape growth dynamics and phenotypic outcomes. Finally, it demonstrates how these materials can be harnessed to fabricate metabolically active constructs that enable fermentation and enhanced ethanol (EtOH) production. Together, the results provide new insight into the design and functional integration of living cells within synthetic matrices, potentially advancing the development of robust, programmable, and scalable biofabrication platforms.

2. REVIEW OF LITERATURE

2.1. Circular bioeconomy: rethinking resources

Unlike traditional economies that rely heavily on finite resources such as oil and gas, the circular bioeconomy builds on renewable biological resources — plants, microorganisms, biomass and organic waste — to produce food, energy, materials, and chemicals, with the aim of closing resource loops and reducing environmental impact. Keeping resources in circulation for as long as possible will help lower carbon emissions and, if implemented at scale, improve overall sustainability (**Figure 1**) [1–3].

In practice, this involves valorising side streams and rethinking waste management: crop residues can be converted into biofuels [4], surplus food reformulated into bioplastics and advanced materials [5,6], organic-rich waste streams into bioelectricity [7,8] and industrial off-gases redirected into microbial production of valuable chemicals [9–11]. In this way, the economy mirrors natural cycles, where outputs of one process become inputs to another, reducing the burden on primary resources, minimising waste and restoring value.

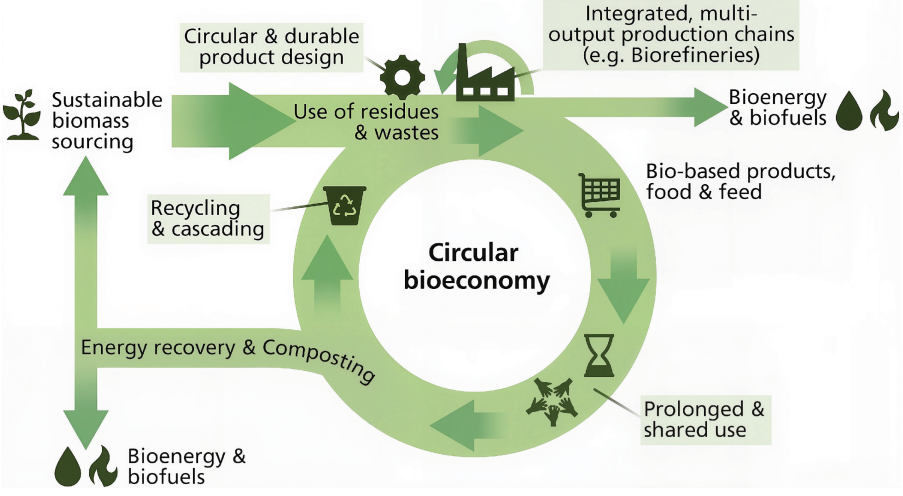

Figure 1. Schematic illustration of the circular bioeconomy and its elements. Adapted from Stegmann *et al.* [1], CC BY 4.0.

Food waste illustrates both the challenge and the opportunity. Globally, millions of tonnes are discarded annually, with a large share ending in landfills, where they generate methane, a potent greenhouse gas [12]. Instead, this biomass can gain renewed value through circular approaches that reintegrate it into new production cycles. Such solutions reduce environmental impact and may even buffer economies against fluctuations in volatile fossil fuel markets.

Achieving this transition requires continuous innovation. Advances in biotechnology, bioengineering, and sustainable design are particularly important, from synthetic biology, which enables the efficient production of bio-based chemicals, to eco-design principles that facilitate recycling and reuse. While the circular bioeconomy sets out the conceptual framework for resource-efficient, closed-loop systems, biomanufacturing (or industrial biotechnology) provides the technological means to realise this vision.

2.2. Biomanufacturing: a shift towards sustainability

The transition to a more sustainable future increasingly relies on biomanufacturing, which harnesses the efficiency of biological systems. Offering practical means to reduce dependence on fossil fuels and to replace conventional chemical processes, which often rely on non-renewable feedstocks and produce hazardous or difficult-to-recycle by-products [13–16]. Within the broader framework of the circular bioeconomy, biomanufacturing serves as a technological foundation for converting renewable feedstocks into a wide range of valuable products.

At its core, biomanufacturing relies on microorganisms and cultured cells — such as bacteria, yeast, algae, and mammalian cells — that act as microscopic factories capable of executing complex biochemical transformations with remarkable efficiency [17,18]. These systems have been successfully deployed across multiple industries. In pharmaceuticals, it underpins the production of biologics such as monoclonal antibodies [19], vaccines [20,21], and therapeutic proteins [22]. Engineered yeast and bacteria have provided an alternative to animal-derived insulin, providing a scalable and reliable alternative [23]. Beyond healthcare, the versatility of bioprocesses has opened pathways to renewable fuels [24], bioplastics [6], food ingredients [25,26], and other high-value materials [27].

The rise of biomanufacturing is inseparable from the advances in biotechnology, genetic engineering, and synthetic biology, which enable the precise design and optimisation of biological systems, improving production efficiency and product yields [25,27–29]. As our ability to reprogram living systems advances, engineered organisms can extend biomanufacturing beyond the inherent limits of natural metabolism, with synthetic biology providing the design principles and toolkits needed to further broaden its scope.

2.3. Synthetic biology and engineered organisms

Conventional biotechnology has long relied on modifying and optimising natural biological processes. Synthetic biology extends these approaches by systematically applying engineering principles — including modularity, standardisation, and abstraction — to design living systems. Its scope ranges from redesigning existing organisms to constructing genetic circuits, logic gates, and orthogonal pathways

[30–33], and increasingly, assembling synthetic genomes and minimal cells to achieve predictable biological functions [30,31].

In this respect, synthetic biology both builds upon and extends the frameworks introduced in the previous sections. The circular bioeconomy provides the conceptual rationale for sustainable, closed-loop systems (Section 2.1), while biomanufacturing operationalises these principles by deploying cells as production platforms (Section 2.2). Synthetic biology complements these approaches by rendering such platforms programmable, thereby expanding the range of products and functions achievable through biological means.

Nevertheless, several critical challenges remain. Technical issues include the genetic instability of engineered traits and limitations in scalability [32–35]. Equally important are the concerns around biosafety and biosecurity, which highlight the need for robust containment and regulatory oversight [36,37]. From a sustainability perspective, large-scale production can impose significant demands on water, nutrients, and energy resources. Furthermore, the high costs of strain engineering, fermentation, and downstream processing continue to limit cost efficiency [33,34]. Ethical and societal factors also shape the trajectory of the field: public acceptance of synthetic biology remains uneven, often echoing controversies around genetically modified organisms [38,39].

Taken together, these considerations suggest that synthetic biology should be viewed not merely as a production tool, but as a design paradigm. Its capacity to equip organisms with new functions underscores the transformative potential and the importance of responsible governance. This trajectory naturally leads into the following section, which examines how biological programmability can be combined with materials science to create engineered living materials (ELMs).

2.4. Engineered living materials: the synergy of biology and materials science

The new and rapidly expanding field of ELMs lies at the intersection of biology and materials science, combining the programmability of living systems with the structural support, tunable mechanics, and environmental resilience of materials. These materials transcend the limitations of inert matter, creating hybrid systems where structure and function co-evolve. Picture a world where man-made materials grow, self-heal, adapt to their environment, and communicate. Walls that capture carbon, textiles that purify the air, and surfaces that glow in response to toxins are no longer confined to science fiction — they are emerging into reality with ELMs [40–42]. This shift is not only technological but also philosophical — it redefines how we relate to the material world, positioning synthetic biology not just as a tool but as a co-designer.

As the field grows, it is increasingly clear that technical advances alone are not sufficient; there is also a need to clarify what is meant by “engineered living material” and where its boundaries lie. This has prompted discussion within the

community about how ELMs should be defined and who gets to define them. Wil V. Srubar III has nicely articulated questions that are on many people's minds: "What constitutes an ELM? Must it contain genetically modified cells to qualify? A synthetic biologist may think so. However, to a materials scientist, every anthropogenic material is engineered to some degree. Discipline-specific terms and definitions are inherently correct, but, for active researchers within the new, interdisciplinary ELM community, the question ultimately remains: whose definitions will prevail?" [43].

This perspective highlights an important point for the present work: ELMs are not defined in a single, universally accepted way, but represent a group of related ideas that different disciplines view differently. In this thesis, therefore, a practical definition of ELMs is provided as materials in which living cells are an integral, active part of the material.

Two complementary design logics have been proposed when designing and developing ELMs [44]. Bottom-up "biological ELMs" (bio-ELMs) leverage cellular production — such as biofilm formation, extracellular protein scaffolds, or biomineralisation — to build constructs autonomously (through self-assembly or growth) from the cell outward [40,45,46]. For example, curli amyloid fibres have been programmed to form functional biofilm-based materials[46], with surface-displayed binding modules that template inorganic components or immobilise enzymes on the fibre surface [47,48]. Biomineralisation has likewise been engineered to drive silica or carbonate precipitation at or beyond the cell surface, yielding mineralised living composites [49–51]. Top-down "hybrid living materials" (HLMs) embed organisms within pre-engineered materials (e.g., polymers, metals, carbons, ceramics and composites) [44], enabling macroscale shaping and immediate control over transport and mechanics [52].

Beyond design tactics, several taxonomies have been proposed to bring order to a diverse literature. One scheme organises the field by scale, design approach, organism, material properties, and application domain — highlighting persistent challenges of scaling from nano/micro to macro while retaining biological function [52]. A complementary framework classifies ELMs by living constituent (domains/kingdoms of life, plus synthetic cells and cross-kingdom consortia) and by material form, introducing "superkingdoms" of bio-ELMs and HLMs (cells + abiotic scaffold), with phyla tied to dimensionality (0D–3D, dynamic, fractal) (**Figure 2**) [44].

This new material paradigm has already moved beyond conceptual proposals into functional prototypes. Applications now span biomedicine (biosensors [53], cell delivery [54], drug-eluting patches [55]), environmental technologies (biosensor for detection of aquatic toxicity [56], mercury bioremediation [57], carbonate-precipitating "living" binders [58]), energy and electronics (microbial fuel cells, biophotovoltaics, living electrodes [59]), and soft robotics and responsive devices [60–62]. Together, these developments demonstrate how ELMs can offer adaptive, self-sustaining functions that conventional engineered materials cannot replicate.

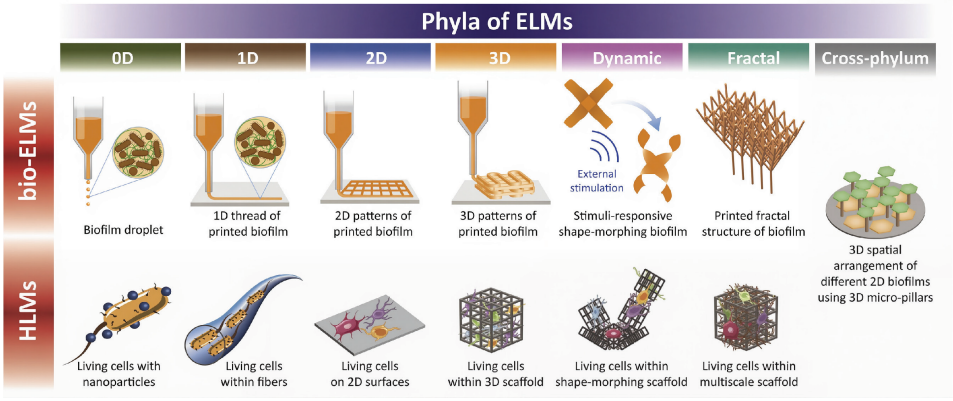

Figure 2. Phylum-level taxonomy of engineered living materials. The schematic highlights representative examples and core concepts for each phylum; these are illustrative rather than comprehensive [44]. CC BY 4.0. Key: bio-ELM – biological engineered living material; HLM – hybrid living material.

Biological systems naturally respond and adapt to their surroundings; therefore, the material must consistently facilitate the efficient diffusion of substrates and products to support the survival, growth, and metabolic activity of these living organisms. There are typically also stringent constraints on the materials' properties at the macroscopic level. The final construct must be manageable, potentially transportable, preservable, reusable, and protective of the embedded cells. Structurally, HLMs are most often based on hydrogels — highly hydrated, crosslinked polymer matrices that provide mechanical support and maintain cellular microenvironments. Hydrogels provide a 3D, water-rich structure that supports microbial viability, permits the diffusion of nutrients, gases, and signalling molecules, and can be engineered over a wide range of stiffness, porosity, and optical properties [63–65], which is why they have become the dominant matrices in the field of ELMs. Both natural (e.g. alginate, chitosan, gelatin, agarose) and synthetic polymers (e.g. polyethylen glycol, polyurethane, and polyacrylamide) are used in ELMs, with crosslinking typically triggered by light, multivalent ions or temperature [66,67].

As research accelerates at the interface of synthetic biology and material science, ELMs provide a practical route to materials that embed biological function aligned with the sustainability aims outlined earlier (Sections 1–2). Realising their full potential requires fabrication strategies that provide the spatial and structural control necessary to design, engineer and scale ELMs with biological complexity and programmable function. The following section explores how 3D printing serves as a powerful enabler of this vision.

2.5. 3D printing: a powerful method for ELM fabrication

3D printing first emerged in 1986 with the development of stereolithography [68], followed closely by extrusion printing in 1988 [69]. Its first application in the field of biology was in 1998, when porous constructs were created using powder bed inkjet printing for culturing hepatocytes [68]. As interest grew almost exponentially, the term "bioprinting" emerged in the early 2000s, with Mironov and colleagues helping to formalise the field in their 2006 review [69]. Bioprinting refers to the precise patterning of biomaterials, cells, and bioactive molecules, enabling the fabrication of bioactive cell-laden matrices and constructs for tissue engineering [67]. While bioprinting mammalian cells has found applications in regenerative medicine [70], drug discovery [71], and disease modelling [72], bioprinting of microorganisms is a relatively recent but rapidly expanding field that has already been used to create functional materials for environmental applications [73], therapeutic devices [74], and bioproduction [75,76]. Compared with mammalian cells, microorganisms exhibit higher resilience, greater tolerance to extreme conditions, and more flexible printing requirements, making them compatible with a broader range of printing technologies [77]; for example, incorporating bacterial spores as the active component allows molten deposition printing at temperatures as high as 75 °C [78].

Although the feasibility of embedding microbial cells within different matrices and printing them using various bioprinting techniques has been demonstrated [77], the mechanistic understanding of how matrix architecture and physical constraints influence cellular physiology remains limited. In particular, the relationships between the mechanical environment, transport properties, spatial confinement and metabolic performance within cell-laden materials are still poorly characterised.

2.5.1. Bioprinting methods

Bioprinted constructs can be fabricated using a range of additive manufacturing techniques, each with its own benefits, limitations, and material requirements. Numerous 3D printing processes have been explored within bioprinting [79–81]. However, given the focus of this thesis on hydrogel-based printing for the development of ELMs, the discussion is limited to four representative approaches directly relevant to cell-laden hydrogels: extrusion printing, inkjet printing, photopolymerisation-based (e.g., stereolithography), and laser-assisted bioprinting. **Figure 3** summarises the core principles underlying each technique, which are elaborated in the following sections.

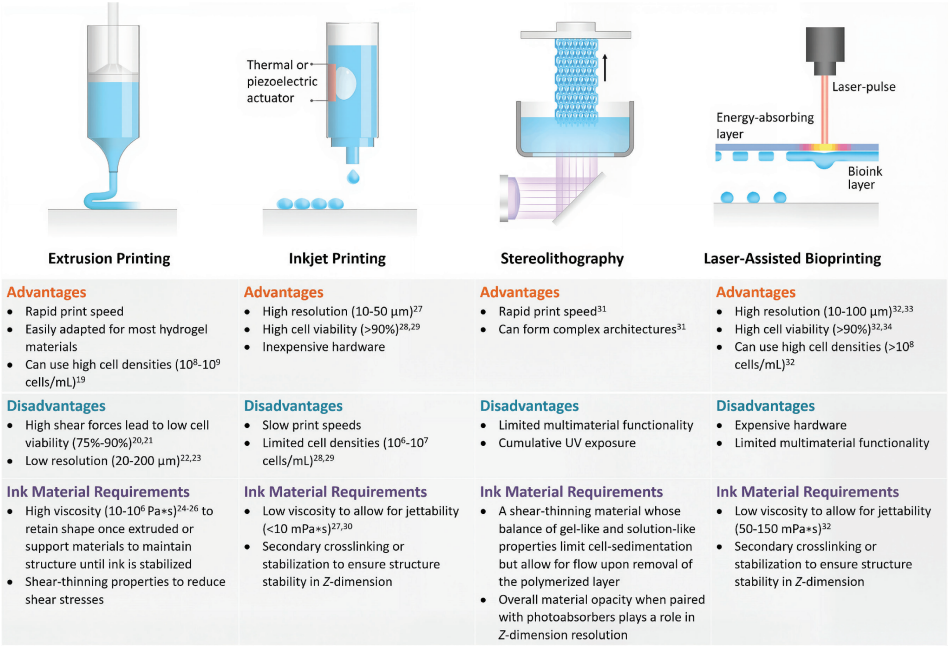

Figure 3. Advantages, disadvantages, and unique components of the most common fabrication techniques used in bioprinting [67]. © 2020 American Chemical Society

2.5.1.1. Extrusion printing

Extrusion printing is one of the most commonly used methods for biofabrication of 3D cell-laden constructs [82]. In extrusion bioprinting, the bioink is typically inserted into a syringe barrel, and the material is dispensed through a nozzle, layer by layer, onto the print surface (**Figure 3**). It can be powered by a piston, screw, or pneumatic pressure. Piston and screw systems provide better control over flow and spatial precision, but create pressure variations that may reduce cell viability [83,84] by potentially disrupting cell membranes [85,86]. Nozzle geometry affects shear stress, with cylindrical nozzles generating more stress than conical ones [87,88]. Extrusion bioprinting supports high cell densities and offers relatively rapid fabrication, making the production of large, cell-laden scaffolds easier. However, the inks used are usually quite viscous to maintain structural stability after extrusion, ranging from 10 to 300 Pa·s [67,89]. Hydrogels are easily adapted to extrusion printing, as they can be extruded directly or printed in a precursor form and stabilised by crosslinking. Ideally, extrusion ink is shear-thinning, which becomes less viscous under shear stress during flow in the nozzle and regains viscosity after deposition to maintain shape [67,86,90]. Non-shear-thinning inks can still work if they rapidly gel or crosslink to stabilise their structure [67].

2.5.1.2. Inkjet printing

Inkjet bioprinting deposits cell-laden droplets onto a substrate using thermal, piezoelectric, or electromagnetic actuation (**Figure 3**). Thermal systems are generally preferred for live cells, as the brief temperature rise (4 to 10 °C for ~2 μs) has a minimal impact on viability [91], whereas piezoelectric actuation can damage membranes at certain frequencies [92]. The technique enables high-resolution patterning with droplet volumes ranging from 10 to 150 pL and precise spatial placement [93–95]. Inkjet bioinks typically have low viscosity (<10 mPa·s) and low shear stress (<10 kPa) to ensure droplet formation and maintain cell viability [67]. However, increased cell loading elevates viscosity and may affect printing precision. Rapid post-printing gelation or crosslinking (e.g., photopolymerisation) is required to prevent spreading and retain structural fidelity, while surface tension must be tuned to ensure controlled droplet formation [96]. Despite these constraints, inkjet bioprinting supports a diverse range of bioinks and enables the accurate fabrication of cell-laden constructs for tissue engineering and regenerative medicine [67,96,97].

2.5.1.3. Photopolymerisation-based (e.g. stereolithography)

Stereolithography (SLA) and related techniques, such as digital light processing and two-photon polymerisation, utilise light-based polymerisation to construct 3D objects from photocurable polymer solutions. In SLA, ultraviolet (UV) light or a laser is directed onto a resin pool to selectively crosslink the material, layer by layer. This allows for high resolution in the X and Y dimensions (10–100 μm), with the Z-axis resolution controlled by managing light absorption within the resin. Digital light processing, an evolution of SLA, projects entire patterned layers at once, increasing printing speed, while two-photon polymerisation achieves submicron resolution for delicate structures by using high-intensity, ultrafast laser pulses [67,97]. Cell viability is generally maintained during SLA, as it lacks mechanical stress on the materials [98], yet biocompatibility is a concern due to the potential cytotoxicity of photoinitiators [99]. These agents, required for polymerisation, may leave behind toxic residues, and UV exposure can damage cellular DNA [100]. Thus, careful selection of light wavelengths, intensities, and photoinitiators is essential. SLA and digital light processing are particularly effective in producing precise, vascularised, and tubular structures (e.g., vascular grafts [101] and nerve conduits [102]), while two-photon polymerisations, with its very fine resolution, is ideal for complex microstructures, such as those in cardiac tissue [103] or the blood-brain barrier [104].

2.5.1.4. Laser-assisted bioprinting

Laser-assisted bioprinting (LAB) utilises a “ribbon” comprising a thin layer of cell-laden bioink over an energy-absorbing material, typically gold or titanium, although alternatives such as gelatin have been explored [105]. A pulsed laser is directed from above, generating rapid local heating and a phase change that propels picoliter droplets of bioink onto the substrate beneath (**Figure 3**). Unlike nozzle-based inkjet systems, LAB avoids shear stress on cells, thereby achieving very high cell viability rates within the produced ELMs [67,105]. The precise laser control and small droplet size enable exceptionally high resolution, including the placement of single cells [106]. However, the requirement for high-precision laser equipment makes LAB substantially more expensive than other bioprinting methods. Suitable bioinks typically have viscosities around 100 mPa·s and require secondary crosslinking to provide structural integrity in the Z-direction [67].

2.6. Copolymers

Copolymers are macromolecules formed by the polymerisation of two or more distinct monomer species. Their defining feature lies in the arrangement and proportion of different repeating units within the polymer backbone, which enables a level of tunability not achievable with homopolymers. By carefully selecting monomers and controlling polymerisation conditions, copolymers can be designed with tailored physical, chemical, or biological properties [107].

Several structural variations of copolymers exist (**Figure 4**). Random copolymers incorporate monomer units in an undefined sequence, whereas alternating copolymers arrange them in a strict one-to-one order. Block copolymers consist of extended sequences of one monomer type linked to blocks of another, resulting in microphase separation and self-assembly into ordered nanostructures. In contrast, graft copolymers feature side chains of one monomer type attached to the backbone of another [108]. More complex arrangements, including gradient copolymers or star-shaped topologies, further extend the design space [109,110].

The broad structural diversity of copolymers supports their versatility across a wide range of applications. In materials science, they are frequently used to modulate mechanical properties, thermal behaviour, and solvent interactions. Amphiphilic block copolymers, such as poloxamers, are particularly notable for their capacity to self-assemble into micelles and gels [111]. This feature underpins their widespread use in drug delivery, tissue engineering, and stimuli-responsive hydrogel systems [112].

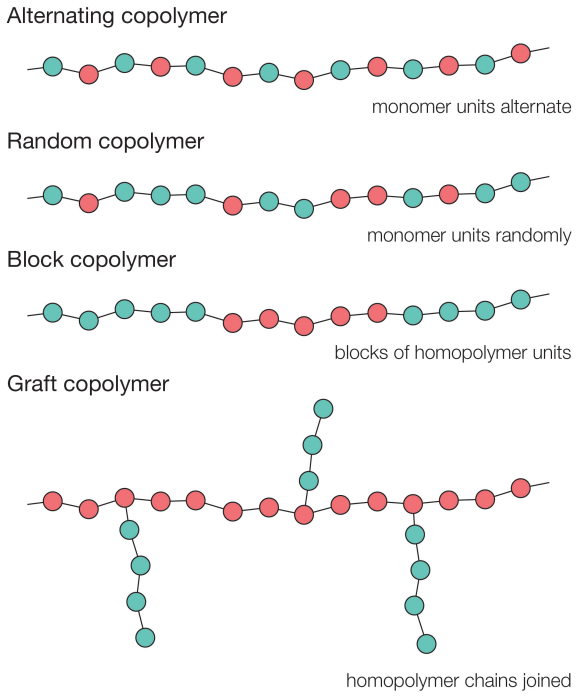

Figure 4. Structures of different types of copolymers.

2.6.1. Poloxamers: micelle formation and mechanism

Poloxamers, commercially known as Pluronics®, were first synthesised by Wyandotte Chemical Corporation in the late 1940s [113], commercialised by BASF around 1950 under the Pluronic® trademark [114], and introduced into biomedical research in the early 1970s [115]. They are defined as non-ionic amphiphilic triblock copolymers with the general structure poly(ethylene oxide) — poly(propylene oxide) — poly(ethylene oxide) (PEO — PPO — PEO). Two "hydrophilic" PEO segments flank the "hydrophobic" PPO block, and the relative block lengths determine the copolymer's solubility, aggregation behaviour, and phase transitions [116]. This versatile yet straightforward architecture has made poloxamers an important model system for studying self-assembly and thermoresponsive behaviour in amphiphilic polymers [117].

Poloxamers exist as individual unimers at low concentrations and temperatures when dissolved in water or aqueous solution. Above specific thresholds of concentration and temperature, they self-assemble into micelles, with PPO blocks forming the hydrophobic core and PEO chains extending into the solvent as a hydrated corona. These thresholds are defined as the critical micelle concentration (CMC) and the critical micelle temperature (CMT). Reported values typically range between 10^{-4} and 10^{-3} M for the CMC and around 10–25 °C for the CMT, depending on the polymer's molecular weight and block composition [118].

Thermoresponsiveness is governed by temperature-dependent hydration equilibria between the PEO and PPO blocks. At lower temperatures, both blocks

remain sufficiently hydrated to favour solubility, whereas increasing temperature drives PPO dehydration and hydrophobisation, leading to micelle formation [118]. This thermoresponsiveness underpins many practical applications of poloxamers, particularly where temperature-triggered gelation or drug release is desirable.

Poloxamers have been extensively investigated due to their biocompatibility, tunability, and reversible sol–gel properties. In pharmaceuticals, they are widely applied as solubilisers for hydrophobic drugs, injectable depots, and controlled-release systems [119]. Beyond the biomedical context, poloxamers also find widespread industrial use in detergency, dispersion stabilisation, foaming, emulsification, lubrication, and the formulation of cosmetics [118]. Their dual ability to form both regular and reverse micelles, combined with their tunable thermal response, has made them a cornerstone of amphiphilic polymer research and an enabling material in diverse applications [117].

2.6.1.1. Poloxamer 407 / Pluronic® F127

Poloxamer 407, also known as Pluronic® F127 (F127), is one of the most widely studied members of the poloxamer family. It is a high-molecular-weight PEO–PPO–PEO triblock copolymer (PEO_{100}–PPO_{65}–PEO_{100}, ~12,600 Da), distinguished by its relatively large hydrophilic fraction, which provides strong solubility and pronounced thermo-responsive behaviour [115]. Concentrated aqueous solutions of F127 undergo reversible sol–gel transitions at near-physiological temperatures, making it attractive as an injectable and easily handled biomaterial [119].

Historically, F127 has been widely employed in biomedical and pharmaceutical applications. It has been studied as a vehicle for drug solubilisation and controlled release, as a stabiliser for proteins and nanoparticles, and as a thermoresponsive gel for injectable depots and topical formulations [120]. It has also been used as a sacrificial template in materials science, for example, in the preparation of mesoporous materials and nanostructured hydrogels [121].

For applications in ELMs, unmodified F127 presents notable limitations. The absence of permanent crosslinking causes it to dissolve gradually in aqueous environments, limiting long-term stability. In addition, reports of cytotoxicity in mammalian systems further reduce its suitability as a durable encapsulation matrix. To overcome these drawbacks, chemically functionalised derivatives such as F127-DMA [75] and F127-BUM [122] have been developed. These modifications enable photopolymerisation and enhance mechanical robustness, establishing a foundation for the F127-based ELMs.

However, beyond establishing structural feasibility, key knowledge gaps remain regarding how these materials shape biological outcomes. In particular, a mechanistic understanding is lacking of how these hydrogels govern cellular proliferation, spatial retention, and polymer–cell interactions within these confined environments. Moreover, nutrient diffusion and the resulting metabolic constraints have not been systematically characterised. These parameters are crucial for enabling stable, high-density microbial populations that are capable of consistent bioproduction within these architected constructs.

3. AIMS OF THIS STUDY

Building on previous work demonstrating the printability of micellar hydrogels as an ELMs platform, this thesis examines how such materials influence the biological behaviour within 3D-printed constructs. In particular, it focuses on how micellar hydrogels influence cell proliferation, spatial retention, explores polymer–cell interactions, and the transport of nutrients and oxygen in confined constructs.

The overall aim of this thesis was to investigate UV-crosslinkable micellar hydrogels as structural and functional matrices for 3D-printed engineered living materials, and to provide foundational insights for developing resilient, sustainable materials for bioproduction.

The specific aims were as follows:

- Characterise synthetic, photo-crosslinkable micellar hydrogels (F127-BUM, F127-DMA, PGE-DMA) as 3D printable matrices for ELMs, and compare their printability, structural fidelity, swelling behaviour and post-printing stability under cultivation conditions.
- Assess the viability and mobility of encapsulated yeast, bacteria, and algae within F127-based matrices, and evaluate their resistance to cross-contamination within and around the hydrogel construct.
- Examine *Saccharomyces cerevisiae* colony proliferation patterns across different micellar matrices to identify differences in cell-matrix interactions and determine how hydrogel mechanical properties influence cell phenotype and relate to cell retention.
- Determine diffusion rates of small molecules in F127-based matrices and evaluate how these micellar matrices affect the metabolic activity and oxygen consumption of encapsulated *Saccharomyces cerevisiae*.

4. MATERIALS AND METHODS

The detailed experimental procedures employed in this thesis are available in the corresponding original publications (I–IV), which provide in-depth protocols for each method applied. This section offers an overview of the key methods used.

4.1. Polymers (I–IV)

Pluronic® F127 dimethacrylate (F127-DMA), Pluronic® F127 bis-urethane methacrylate (F127-BUM), and poly(isopropyl glycidyl ether-stat-ethyl glycidyl ether) — poly(ethylene oxide) — poly(isopropyl glycidyl ether-stat-ethyl glycidyl ether) dimethacrylate (PGE-DMA) were supplied by the Nelson Laboratory (University of Washington). The synthesis of these polymers has been described in detail in the laboratory's previous publications [75,122,123]. The degree of functionalisation was 81% for F127-DMA, whereas F127-BUM and PGE-DMA were functionalised quantitatively. The chemical structures and their temperature-induced micelle formation are illustrated in **Figure 5**. The polymer formulations and working concentrations used in this thesis are summarised in **Table 1**.

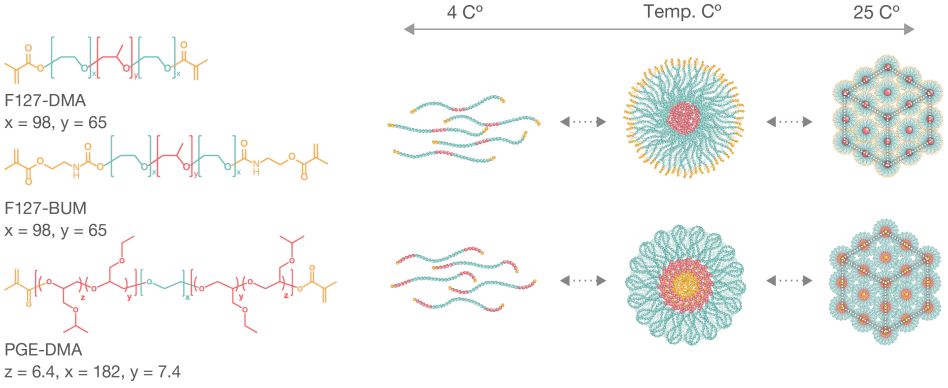

Figure 5. Chemical structure of copolymers used and thermo-responsive behaviour of the polymers due to micelle formation.

Table 1. Polymer concentrations used in this thesis.

Polymer	Full name (descriptive)	Publications/concentrations (w/w)
F127-BUM	Pluronic F127–bisurethane methacrylate	**I:** 30% • **II:** 30% • **III:** 30% • **IV:** 20%, 25%, 30%
F127-DMA	Pluronic F127–dimethacrylate	**I:** 30% • **IV:** 30%
PGE-DMA	PGE–PEO–PGE dimethacrylate triblock copolymer	**I:** 20% • **IV:** 20%

4.2. Hydrogel preparation for 3D printing (I–IV)

Sterile 0.1 M PBS was added to the polymer, and the mixture was stirred on ice with a magnetic stirrer until the polymer was completely dissolved. For printing, 1–2 µL g^{-1} of the photoinitiator 2-hydroxy-2-methylpropiophenone (Irgacure 1173, >97%, Sigma-Aldrich) was added and stirred on ice for 30 minutes. For experiments with cells, 10^5–10^7 spun-down cells g^{-1} hydrogel were mixed in for 5–10 min and then incubated on ice for 30 min to remove bubbles. The solution was transferred to a 10 mL dispensing barrel with a 0.41 mm conical syringe tip and brought to room temperature before printing.

4.3. Microorganisms across publications (I–IV)

Microorganisms used in Publications I–IV include several microbial strains. **Table 2** summarises the microorganisms used, their strains and their experimental roles.

Table 2. Microorganisms and strains used in Publications I–IV and their primary roles in this thesis.

	Microorganism	Strain	The main purpose of the study
I	*Saccharomyces cerevisiae* (yeast)	CEN.PK113-7D (MATa, MAL2-8c, SUC2)	An EtOH-producing organism to examine how physical confinement in different micellar matrices affects colony morphology, cell size, immobilisation, and apparent matrix degradation/remodelling.
II	*Saccharomyces cerevisiae* (yeast)	yJS001 (SO992; mfa2::pTEF1_mCherry; kanR)	Strain exhibiting red mCherry fluorescence, used to demonstrate yeast viability and spatial retention in 3D-printed F127-BUM ELMs and to visualise potential cross-bleeding at multikingdom interfaces.
II	*Escherichia coli* (bacterium)	CD02 (MG1655; nfsA::BBa J23119-sfGFP; kanR)	Strain exhibiting green sfGFP fluorescence, used to assess bacterial compatibility with F127-BUM, visualise spatial segregation in co-printed constructs, and monitor suppression of invasion from the surrounding medium.
II	*Chlamydomonas reinhardtii* / *Chlorella* sp. (algae)	Lab strain (not further specified)	Demonstrate the integration of a photosynthetic microorganism in multikingdom 3D-printed ELMs with sustained viability.

	Microorganism	Strain	The main purpose of the study
III	*Saccharomyces cerevisiae* (yeast)	CEN.PK113-7D (MATa, MAL2-8c, SUC2)	Probe oxygen diffusion and metabolic state inside ELMs versus suspension, and demonstrate metabolic bias toward fermentation.
III	*Saccharomyces cerevisiae* (yeast)	Bry-97 beer yeast (Lallemand)	Proof-of-concept 3D-printed brewery, comparing EtOH yield and product quality between ELM-based and classical brewing under oxygen-restricted conditions.
IV	*Saccharomyces cerevisiae* (yeast)	CEN.PK113-7D (MATa, MAL2-8c, SUC2)	Provide yeast-laden micellar hydrogels as an experimental counterpart to the *in silico* simulations.

4.4. 3D printing

3D printing was conducted using a K8200 printer (Velleman, Belgium) modified for direct pressure dispensing [I, III, IV] or a modified Tronxy P802E (Shenzhen Tronxy Technology Co., China) for pneumatic dual extrusion [II]. The computer-aided design (CAD) model was created with SolidWorks (Student Edition), and G-code was generated using the open-source 3D printing software Slic3r (version 1.3.0). For pneumatic dispensing, the generated G-code was modified using Python to incorporate the necessary solenoid switching commands.

4.5. UV-polymerisation (I–IV)

The hydrogels were polymerised for 60 to 180 s with four light-emitting diodes (CUN66A1B, Seoul Viosys, Republic of Korea) emitting at 365 nm wavelength.

4.6. Cell viability testing (II)

After printing and curing, the cell-laden hydrogels were incubated in growth media selected according to the embedded species. Samples were maintained at 30 °C under gentle agitation, and the medium was exchanged every 24 hours to ensure a continuous supply of nutrients. Viability was probed after 1, 3, and 7 days of incubation. At the imaging intervals, a small cross-section was cut from the construct for staining. The Sytox Green stain stock solution was diluted to a final concentration of 5×10^{-6} M, and 20 µL of the diluted dye was added to the cut hydrogel sample for 5 minutes. Samples were then gently washed to remove excess stain and imaged using a Leica SP5 confocal microscope.

4.7. Swelling properties (IV)

For characterising swelling behaviour, all 3D-printed hydrogel samples used for the tensile and compressive strength testing were weighed. The initial dry polymer mass employed for hydrogel preparation was considered the starting point (W_P). Following the photopolymerisation, the hydrogels were promptly weighed, obtaining W_{0h}. Subsequently, hydrogels were incubated in a PBS buffer at room temperature (24 ± 1 °C) for 24 hours (providing W_{24h} — the resulting weight, considering non-gel fraction). For temperature-induced swelling investigations, a larger sample with a diameter of 51 mm and a height of 8 mm was cast and UV crosslinked. Changes in mass, polymer concentration and Shore E hardness were measured at various temperatures (5, 10, 15, 20, 25, 30 and 37 °C). These hydrogels were swollen for approximately 72 hours to account for the significantly larger size. No gradients in swelling or optical properties were observed in the swollen samples, indicating uniform polymerisation. Constant temperature was maintained using a thermostat (RP 1845, Lauda, Germany). Before each measurement, the surface moisture of each hydrogel sample was eliminated with a tissue paper. Polymer concentrations of the hydrogels and swelling ratios were calculated using equations (1) and (2), respectively.

$$Polymer\ concentration\ (\%) = \frac{W_P}{W_{0h\ or\ 24h}} \times 100 \quad (1)$$

$$Swelling\ ratio\ (\%) = \frac{W_{0h\ or\ 24h} - W_P}{W_P} \times 100 \quad (2)$$

4.8. Mechanical characterisation (IV)

4.8.1. Tensile strenght

Dogbone samples for the tensile tests (ASTM D412 A: 50% scale, see **Figure A1A**) were fabricated using 3D printing. The dogbone dimensions were assessed using a digital calliper (711, Gedore, Germany) before and after swelling in 0.1M PBS for 24 hours. Tests were conducted in a PBS-filled water bath connected to a universal testing machine, featuring a digital force gauge sensor (FH 500EXT, Sauter GmbH, Germany, as shown in **Figure A1B**), at 24 ± 1 °C. Tensile measurements were conducted at a crosshead speed of 1 mm min^{-1} and the elongation of the gauge section was measured using an in-water bath line gauge. Each material was evaluated using 3–5 independent samples.

4.8.2. Compressive strength

The compressive strength of 3D-printed cylinder samples, measuring 10 mm in diameter and 6 mm in height (before swelling), were evaluated using a universal testing machine equipped with a digital force gauge sensor (FH 500EXT, Sauter

GmbH, Germany) at 24 ± 1 °C and with a crosshead speed of 1 mm/min. Before and after swelling in 0.1M PBS for 24 hours, the sample dimensions were measured using a digital calliper (711, Gedore, Germany). Each polymer type was tested with 3 independent samples.

4.8.3. Shore hardness

Shore A and E hardness testing followed the guidelines outlined in ASTM D 2240 — 15 standard, utilising digital Shore A and E hardness testers (China) calibrated to the standard. To mitigate creep effects, a dwell time of 1 second was employed. Testing was conducted at a temperature of 24 ± 1 °C, unless stated otherwise. Measurements were taken at regular intervals, at least 6 mm from the specimen's edge and 10 mm apart. To measure Shore A hardness, the tensile strength samples were assembled by stacking multiple layers to achieve the required thickness. Shore E hardness was measured alongside temperature-induced swelling, with sample parameters detailed in the corresponding methods section. Each specimen underwent a minimum of five readings, from which the mean was calculated.

4.9. Diffusion studies (IV)

The experimental setup was constructed according to the requirements of the diaphragm cell method to determine the diffusion coefficients of EtOH and glucose in the 3D-printed F127-DMA membrane. One side of the membrane had a solution of EtOH, glucose and formaldehyde (5% /5%/0.5% respectively) in PBS, and the other side had a zero solution (PBS, formaldehyde 0.5%). Formaldehyde was added to the solutions to halt the growth of any living organisms that could affect the test results. Experiments were conducted at 10, 15, 20, 25, 30 and 37 °C with 2–3 independent repeats, and the diffusion coefficient was calculated over more than 10 data points.

The experimental setup (**Figure 6A**) consisted of a large reactor (500 mL), mini-reactors (3×), tubing, centrifuge tubes (50 mL), a peristaltic pump (Ismatec Reglo ICC), a cryostat (Lauda Proline1845), a magnetic stirrer and a power supply. The mini-reactors that held the membrane were designed and flow-optimised using 3D CAD design and flow simulation software (Dassault Systèmes SolidWorks, Figure 6B) and 3D printed on a desktop SLA 3D Printer (Formlabs Form 2). The mini-reactor with F127-DMA membrane, tubing and centrifuge tube formed a closed loop (media volume 35 mL) where the solution was circulated with a peristaltic pump (10 mL min^{-1}). The membrane-containing mini-reactors were placed inside the large reactor, which was filled with EtOH and glucose solution and stirred with a magnetic stirrer. To maintain the specified temperature, the setup was placed in a cryostat water bath.

The experimental setup was sterilised with 70% EtOH and air-dried in a laminar flow cabinet; afterwards, it was irradiated with UV-C light for 3 minutes. The

membranes and solutions were brought to the desired temperature overnight, and membrane thicknesses were measured between two glass slides before the experiment with a digital micrometre (Mitutoyo, Series 293, Japan). After assembling the experimental setup, it was placed in a water bath cryostat pre-set to the required temperature. The first sample was taken 10 minutes after starting the experiment to ensure that any residual EtOH from sterilisation had been flushed out of the tubing. The experiment lasted for 5 hours, with 1 mL of samples taken every hour from each mini-reactor loop. The changes in volume were taken into account during calculations. All collected samples were filtered through a 0.2 µm filter into clean Eppendorf tubes and stored in a freezer (–20 °C) until high-performance liquid chromatography (HPLC) measurements. HPLC measurements were carried out using a Shimadzu Prominence-i LC-2030C Plus 3D machine equipped with a 00H-0130-K0 column.

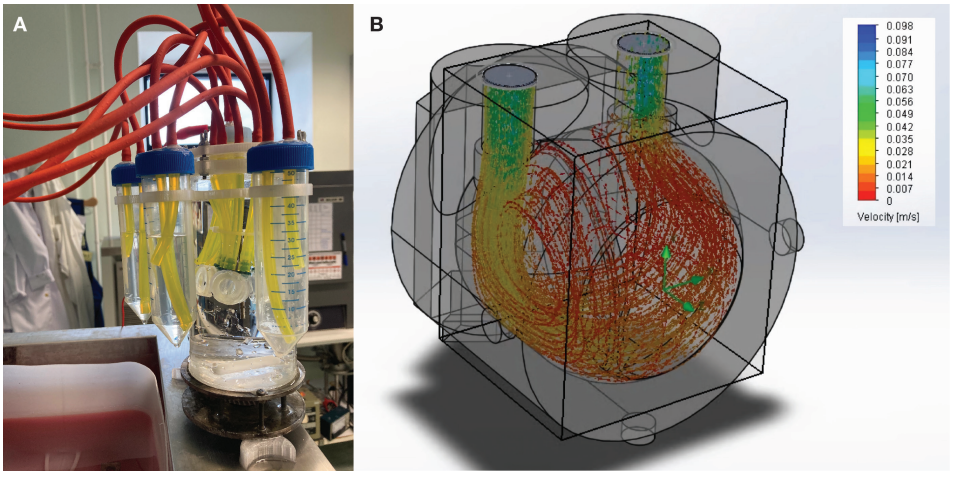

Figure 6. The experimental setup for diffusion studies consisted of three independent small reactor loops, each equipped with a hydrogel membrane submerged in a large reactor with a magnetic stirrer (A). Additionally, a small reactor flow simulation was used for flow path optimisation (B) [IV].

4.10. Scanning electron microscopy (SEM) (I, II, IV)

SEM imaging was conducted using a Hitachi TM3000 (Japan) following the procedures outlined in Publication II. A detailed step-by-step procedure is also accessible as a published protocol [124]. Briefly, samples were fixed in 3.7% formaldehyde in 0.1 M phosphate buffer for 48 hours. Dehydration was performed using an ascending EtOH series (40%–99.5%), with each step lasting at least 2 hours and the final step conducted overnight. Afterwards, EtOH in the samples was replaced with liquid CO_2 in a critical point dryer (E3100, Quorum Technologies, United Kingdom) through 6–8 purging cycles. The critical point was reached by increasing the temperature to 37 °C while maintaining a pressure

of less than 110 bar. The pressure was then released slowly overnight to preserve sample integrity. Dry samples were frozen in liquid nitrogen and cut with a scalpel to obtain artefact-free cross-sections. The cut samples were mounted on stubs with carbon tape and coated with a 7.5 nm gold layer using a high vacuum sputter coater (EM ACE600, Leica Microsystems, Germany). Gold-coated samples were imaged using a tabletop SEM (TM-3000) at 15 kV under a high vacuum.

4.10.1. Image analysis (I)

SEM images were analysed in GIMP and MATLAB R2019b (Image Processing Toolbox). Yeast cells were modelled as ellipsoids for cell-volume estimation (μm^3). Cells were manually outlined in GIMP to generate segmentation masks, which were imported into MATLAB. From these masks, the major (length) and minor (width) axes were extracted, and the third axis (height) was assumed to be equal to the minor axis. Cell volume was then calculated using the ellipsoid volume formula.

5. RESULTS AND DISCUSSION

5.1. Structural precision, patterning capability, and stability of printed micellar hydrogels

Before discussing cellular behaviour within these ELMs, it is first necessary to establish the printability, dimensional stability, swelling behaviour, interface integrity, and baseline stability under cultivation conditions. Together, these results establish the structural and operational envelope within which corresponding ELMs can be designed, printed, and evaluated in bioproduction-relevant settings [I, II, IV].

5.1.1. Printability and structural precision

Establishing the printability and structural stability of the micellar hydrogels was a critical step before assessing their biological performance. All tested polymer hydrogels (**Figure 5**, **Table 1**) demonstrated excellent shape fidelity during 3D printing and retained their structural integrity following photopolymerisation. Notably, 20 wt% F127-based hydrogels required printing at an elevated temperature (~30 °C, using a heated build platform) to preserve gelation upon extrusion, as lower polymer concentrations increase the critical gelation temperature [125]. Other printing parameters remained constant across formulations, aside from minor flow rate adjustments to compensate for concentration-dependent viscosity variations. These observations align with the previously reported shear-thinning and rapid gelation behaviour of these micellar hydrogels [75,122,123], enabling well-defined, geometrically complex features, including overhangs (**Figure 7**). Collectively, these rheological characteristics offer substantial design flexibility for producing constructs with optimised surface area and flow dynamics. Because post-printing hydration can compromise as-printed precision, the next subsection quantifies swelling and its dimensional consequences.

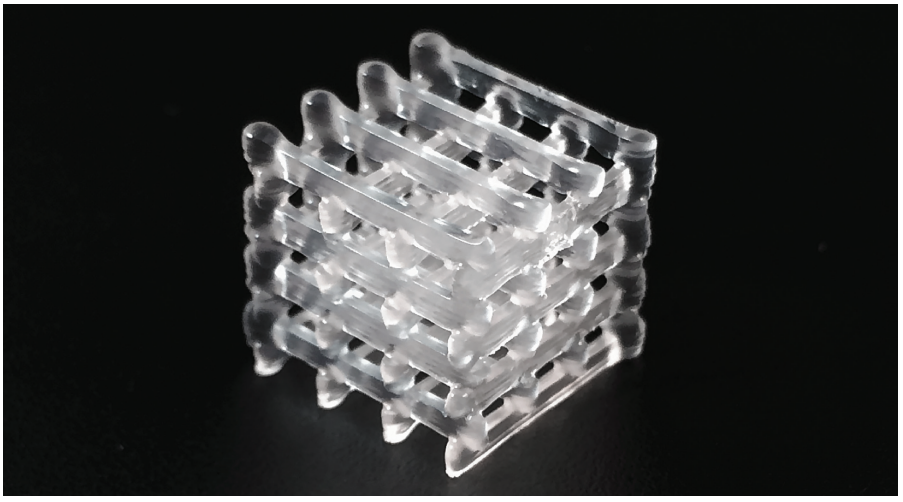

Figure 7. 3D-printed geometrically complex construct based on F127-DMA.

5.1.2. Swelling and equilibrium water content

The water content of printable hydrogels presents a functional trade-off: higher water improves flow and supports cell viability during bioprinting [126,127], whereas lower water content increases the density of polymerisable groups per unit volume, yielding a more crosslinked and mechanically robust network [128]. While this enhances structural integrity, it may reduce flexibility and biocompatibility. Thus, the optimal formulation depends on the intended use — whether prioritising printability and cell survival during fabrication or mechanical stability during operation.

Swelling analysis at room temperature revealed that post-printing swelling decreased with decreasing initial polymer concentration (**Figure 8A**). All hydrogels converged to a similar swollen-state polymer content of ~16–20% (**Figure 8B**), indicating an intrinsic equilibrium water content characteristic of these micellar hydrogel matrices. Thus, initial polymer concentration influences — but does not fully dictate — equilibrium hydration. Highlighting that, in these amphiphilic, long-chained, and flexible micellar architectures, crosslinking functional groups alone cannot overcome hydration forces.

From an engineering standpoint, post-swelling must be accounted for when designing and producing these hydrogels for industrial use, where consistent dimensions are critical (**Figure 8C**). Notably, the observed swelling behaviour also creates scope for shape-morphing designs by strategically patterning polymer concentration within the construct, suggesting potential in adaptive soft robotics and targeted drug delivery. Given the temperature sensitivity of micellar hydration, thermo-modulated swelling and mechanics are examined next.

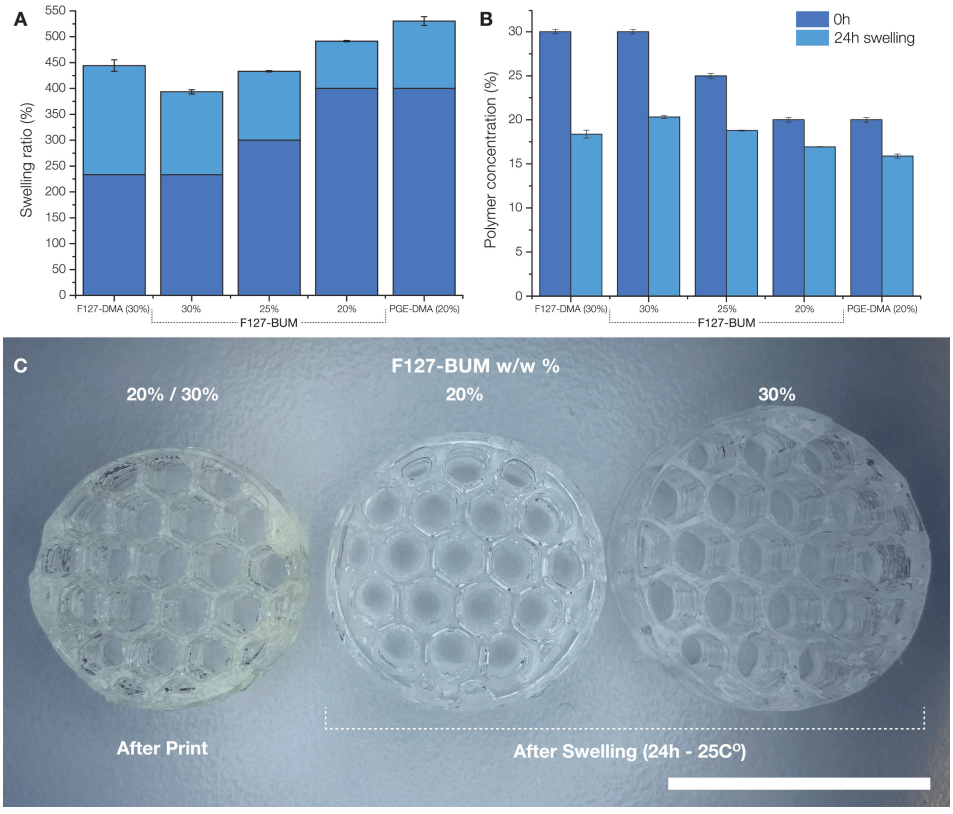

Figure 8. 3D-printed hydrogel samples: swelling ratio (A), polymer concentrations (B), and size comparison (C) illustrate 3D-printed constructs directly after printing and after 24 hours of swelling (scale bar: 20 mm) [IV].

5.1.3. Temperature-induced swelling

F127 is a well-established thermosensitive triblock copolymer [129]; however, quantitative data on temperature responses in its UV-polymerised hydrogel counterparts have been lacking. The relationship between swelling and Shore E hardness was investigated in a 30% F127-DMA hydrogel, which was selected for its superior long-term stability compared to F127-BUM, as discussed in Section 5.5.

The crosslinked micellar matrix of F127-DMA retained its reversible thermo-responsive behaviour (**Figure 9**). Between 10–25 °C, the hydrogel exhibited a significant reduction in water content, leading to an increase in effective polymer concentration. Shore E hardness strongly correlated with these changes, providing a practical, non-destructive proxy for rapid assessment of hydrogel mechanics.

These findings clarify the interplay between temperature, water absorption, polymer content, and mechanical behaviour in crosslinked micellar hydrogels. From a bioproduction perspective, such thermo-responsiveness could offer additional control over diffusion and process rates by modulating the polymer matrix density.

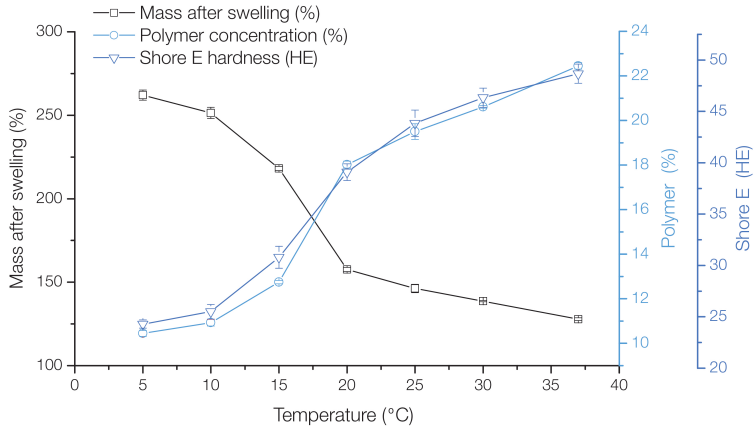

Figure 9. The reverse thermo-responsive behaviour of F127-DMA: total mass after swelling, equilibrium polymer concentration, and Shore E hardness as a function of temperature [IV].

5.1.4. Spatial patterning and interface integrity

Leveraging CAD with a multi-material direct-write 3D printing platform enabled the precise deposition of discrete microbial populations — *Saccharomyces cerevisiae* (yeast), *Chlorella vulgaris* (algae), and *Escherichia coli* (bacteria) — into adjacent compartments within a single construct (30 wt% F127-BUM). All bioink formulations shared the same base hydrogel chemistry and differed only in the embedded microorganism, enabling cross-polymerisation at interfaces and contributing to overall structural coherence. The printed bioinks maintained sharp boundaries in all tested configurations with no observable microbial cross-bleeding between zones. This demonstrates that high spatial resolution and biological modularity can be sustained irrespective of microbial type within the established printability and swelling limits. Given the demonstrated printability of all formulations, it is reasonable to expect each formulation to support the fabrication of such multi-kingdom consortia with comparable patterning performance. To enable the interpretation of subsequent ELM experiments, baseline stability in the absence of cells was first established and is discussed in the following section.

5.1.5. Acellular stability under cultivation conditions

Prior to biological experiments, acellular crosslinked hydrogels were incubated for 14 days in culture media to establish baseline stability. The controls appeared stable at both macroscopic and microscopic levels under physiological conditions (**Figure 10**); no creep was observed in any sample across the cultivation period. The surrounding medium showed no detectable changes in glucose concentration or pH, and the mass of the control constructs remained unchanged. These acellular data provide the reference against which structural transformations in cell-

laden hydrogels — arising from proliferation or metabolic activity — can be interpreted in the subsequent sections.

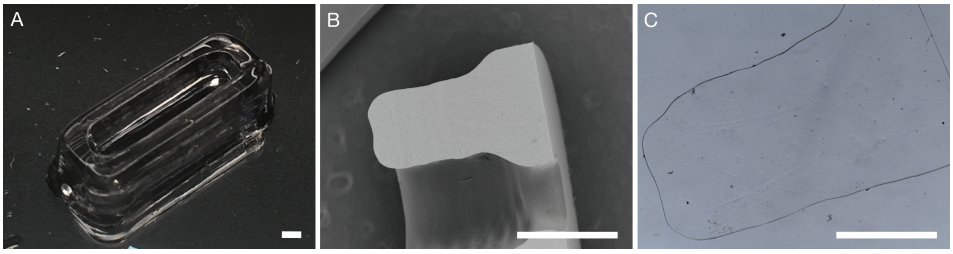

Figure 10. Illustrative images of control constructs (hydrogels printed without cells). Photograph after 24 h equilibration (A). Cross-sectional scanning electron microscopy (SEM) micrograph (B). Optical microscopy (OM) micrograph; slice thickness 40 μm (C). Scale bar is 1 mm [I].

5.2. Cell viability in micellar hydrogel ELMs

Before proceeding to biofunctional demonstrations, the biocompatibility and cell viability of the cell-laden hydrogel matrix was evaluated to ensure that it can sustain embedded living cells after printing. Because unmodified F127 lacks long-term stability and gradually dissolves under aqueous conditions [67], its crosslinkable derivative, F127-BUM, was selected as a representative system for assessing cell viability. Three microbial species — *Escherichia coli*, *Chlorella vulgaris*, and *Saccharomyces cerevisiae* (**Table 2**) — were employed as model organisms, referred to as B-ink (bacteria), A-ink (algae), and Y-ink (yeast), respectively. These bioinks were used to produce spatially defined constructs containing paired microbial combinations (AY, BY, and BA), allowing for the assessment of single-species viability and cross-species compatibility within a shared matrix architecture.

Post-printing viability evaluation confirmed high biocompatibility of the F127-BUM hydrogel. All three embedded species maintained viability around 90% over a 7-day incubation (**Figure 11**), demonstrating that the crosslinked F127-BUM network supports metabolically active cells without detectable cytotoxic effects. Thus, F127-BUM hydrogels can maintain the viability of these different microbial strain combinations, and is also suitable for consortia studies.

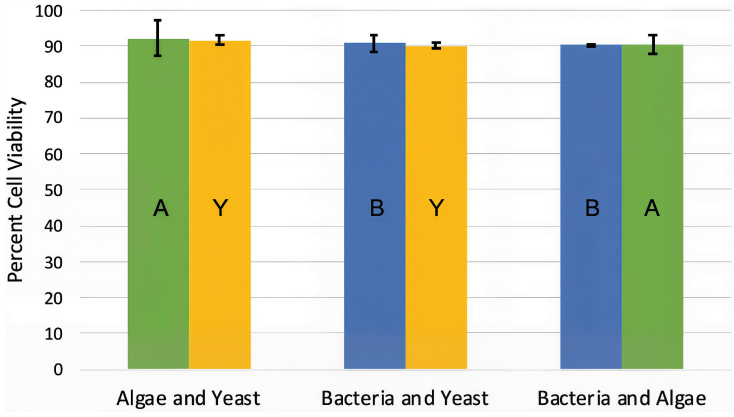

Figure 11. Cell viability results from 7 days of incubation in coculture. During a week of incubation in mixed cell culture medium, all cell types show high viability when encapsulated in the cured F127-BUM hydrogels at an initial loading of 10^7 cells g^{-1}. "A" represents algae, "B" represents bacteria, and "Y" represents yeast [II]. © 2020 WILEY-VCH Verlag GmbH & Co. KGaA, Weinheim

5.3. Microbial Co-Localisation and Spatial Retention in micellar hydrogel ELMs

Following the confirmation of matrix biocompatibility, the capacity of cross-linked F127-BUM hydrogels to retain embedded cells and maintain spatial organisation was examined. During incubation, a gradual release of cells into the surrounding aqueous medium was observed, primarily attributable to cells located at or near the hydrogel surface. This behaviour suggests that a short post-processing step to generate a cell-free peripheral layer could enhance long-term cell retention.

Microscopic analysis showed that discrete microbial populations remained confined within their printed compartments, maintaining sharp interfaces without measurable migration across boundaries. Occasional bacterial adhesion to the external surface was observed, yet no penetration into the matrix or movement between neighbouring regions occurred throughout the observation period (**Figure 12**). These findings demonstrate that the micellar hydrogel matrix provides both mechanical support and spatial containment, thereby sustaining the designed architecture of multi-kingdom assemblies.

The combination of physical confinement and diffusional permeability renders the F127-BUM hydrogel an effective selective barrier that limits microbial diffusion while preserving nutrient transport essential for metabolic activity. By resisting colonisation from the surrounding medium and preventing intermixing between embedded populations, it provides a well-defined, controllable microenvironment. This compartmentalisation allows genetically or functionally distinct microorganisms to be co-localised within a single construct without uncontrolled

competition. Together with its ease of patterning and high biocompatibility, F127-BUM enables consortium designs and applications that are difficult to achieve with other existing materials or liquid culture schemes.

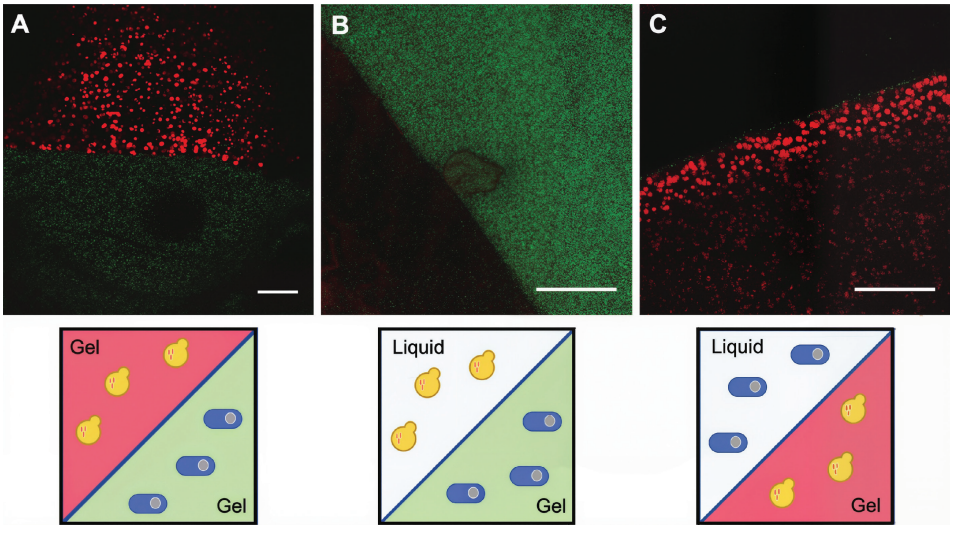

Figure 12. Micrographs of multimaterial 3D-prints. (A) The interface of a hydrogels containing green fluorescent bacteria (green) and red fluorescent yeast (red) (**Table 2**), across 100 µm of sample depth. (B) Sample of bacteria-laden hydrogel printed and incubated in yeast culture. (C) Sample of yeast-laden hydrogel printed and incubated in bacterial liquid culture. Images shown after 7 days of co-culture. Scale bars are all 100 µm [II]. © 2020 WILEY-VCH Verlag GmbH & Co. KGaA, Weinheim

5.4. Cellular growth, retention, and phenotype in micellar hydrogel ELMs

After establishing that triblock copolymers are readily patternable and capable of supporting the viability of diverse microbial populations, the next logical step was to examine in greater detail how and where living cells grow within these matrices, and whether noticeable differences emerge between different hydrogels in terms of proliferation patterns, cell retention, colony morphology, polymer–cell interactions, or cellular characteristics.

To investigate these aspects, *Saccharomyces cerevisiae* were encapsulated within three distinct triblock copolymer hydrogels: F127-DMA, F127-BUM, and PGE-DMA (**Table 1**). To prevent contamination of the culture medium by peripheral cells from the outset, all samples were post-treated with 70% EtOH immediately after UV curing, creating a cell-free zone around the periphery [I].

5.4.1. Proliferation patterns

After one week, apparent differences were observed in how *Saccharomyces cerevisiae* grew within each hydrogel, and these distinct proliferation patterns remained largely stable during the second week. The most pronounced differences appeared in peripheral regions. In F127-based hydrogels, peripheral colonies merged and gradually formed a continuous film that expanded outward over time (**Figures 13A, B, D, E**), while the constructs' interiors remained comparatively compact. In some F127-DMA samples, cell-free and cell-laden regions were completely separated (**Figure A2**). By contrast, colonies in PGE-DMA constructs grew preferentially toward the periphery, and no distinct separating layer formed as observed in F127-based ELMs (**Figures 13C, F**).

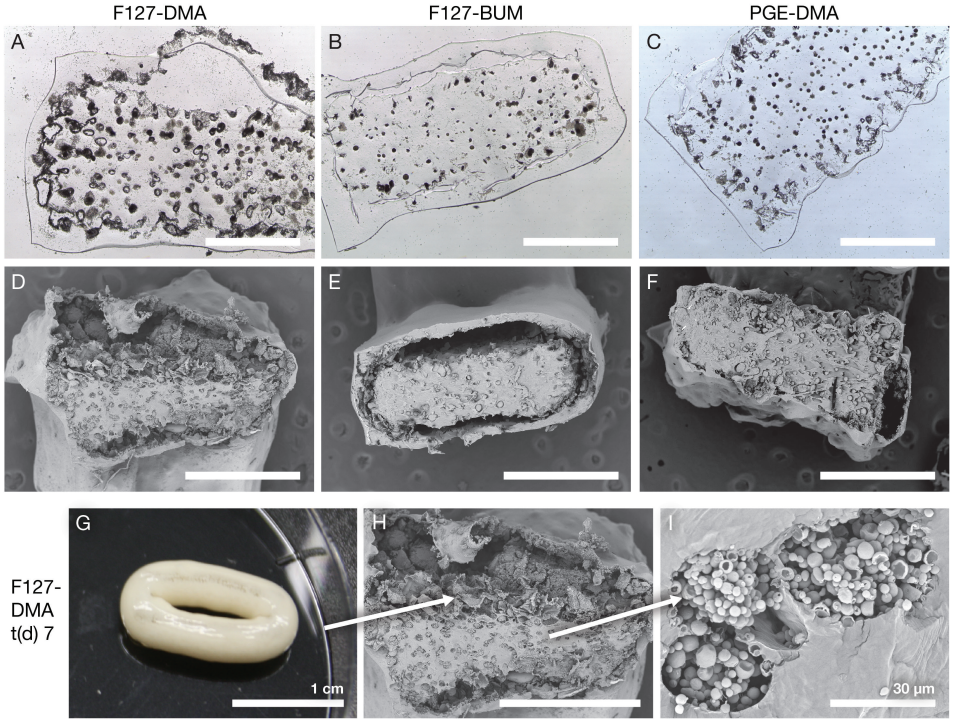

Figure 13. Optical microscopy (OM)(A−C) and scanning electron microscopy (SEM)(D−F, H, I) micrographs of engineered living materials (ELMs) after 7 days of incubation. Cells escaped from PGE-DMA, without major disruption of the material, F127-DMA, and F127-BUM formed separated layers (center vs. shell). Most cell proliferation occurred at the interface. The ELMs swelled up and retained cells up to a particular cell number (G). As peripheral colonies joined into one major colony (G, H), the colonies residing in the middle of the hydrogel were deprived of access to nutrients, causing cell death in colonies (I). Scale bar is 1 mm unless marked differently [I].

A consistent colony size gradient was observed across all hydrogel formulations, with smaller colonies located in the central regions and progressively larger ones toward the periphery. Colony diameters in the central zones remained within the 26–38 μm range throughout the experiment, highlighting the consistency of this spatial pattern across all hydrogel formulations. This spatial distribution is likely driven by nutrient limitations. Diffusion through the polymer matrix is restricted, giving peripheral colonies preferential nutrient access and enabling faster growth. As these populations expand, they progressively consume more available substrates, further limiting diffusion into deeper zones. Eventually, nutrient penetration to the core becomes negligible, eventually leading to cell death within these colonies (**Figure 13I**).

Although thicker constructs could, in principle, host more cells, simply increasing the cross-section does not lead to higher fermentation. Cells in the core become diffusion-limited: nutrient and oxygen supply, as well as waste removal, are restricted, which suppresses metabolic activity. The inactive core is not wasted, however. It provides long-term mechanical support for the overall construct. More broadly, these results indicate that, in these ELM constructs, production performance is limited less by absolute cell loading and more by nutrient and product transport through the matrix, in line with classical Thiele and Damköhler frameworks where geometry and mass transfer, rather than catalyst amount alone, dominate performance in immobilised systems [130,131].

5.4.2. Retention and matrix carrying capacity

The duration for which *Saccharomyces cerevisiae* was retained within the hydrogel matrix varied significantly among materials. F127-DMA exhibited the longest retention time (5.13 ± 1.55 days), followed by F127-BUM (3 days) and PGE-DMA (2 days). Although F127-DMA and F127-BUM share the same polymer backbone and micellar architecture, their retention performance diverges. F127-BUM, with its higher storage modulus and greater degree of functionalisation [75,122], allows earlier cell escape. This outcome suggests that additional parameters — such as material toughness, fracture resistance, and critical strain at break (i.e., how readily cracks propagate once initiated by a growing colony) may also play important roles in determining when and how cells escape.

Hydrogel swelling due to cellular proliferation was evident after 7 days of incubation (**Figure 13G**), with F127-DMA and F127-BUM showing significant mass increases of 136.8% and 53.4%, respectively, while PGE-DMA increased by only 41.28%. Interestingly, by the end of the second week, all hydrogels converged to similar mass gain values (~40%), suggesting that the different formulations ultimately reached a comparable carrying capacity under the applied cultivation conditions (**Figure 14**). This loss of mass resulted from cells escaping from the hydrogels, as they were continuously washed out from the cavity between the inner and outer layers of the F127-based materials. However, since

PGE-DMA did not form such cavities, its weight stayed the same during the second week.

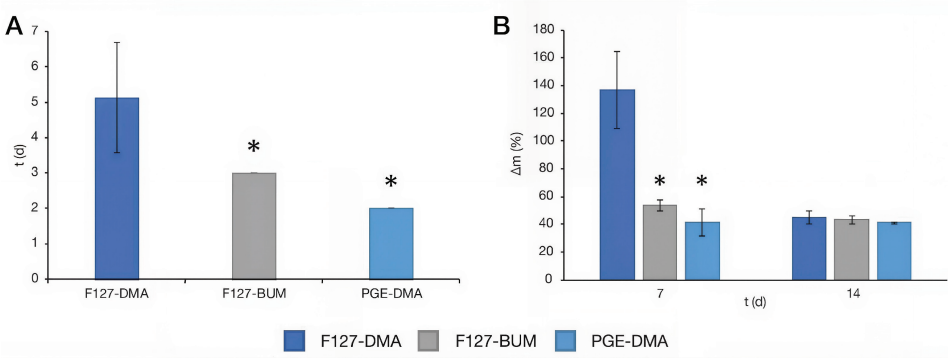

Figure 14. *Saccharomyces cerevisiae* cell retention time (A). ELM mass differences from the starting day to day 7 and 14 (B). * $p < 0.05$, significant difference from F127-DMA. Key: d- day; t- time. The different hydrogel formulations are listed in **Table 1**, adapted from Figure S2 [I].

5.4.3. Colony morphology and growth dynamics

Lower initial cell loading (~10^5 cells g^{-1} hydrogel) and a shorter observation period allowed for the characterisation of a single colony. Within 48–72 hours, colony morphologies diverged across materials. Colonies in F127-based materials were predominantly spherical (**Figures 15A, B, D, E**), while PGE-DMA facilitated more irregular, spindle-like or elliptical growth geometries (**Figures 15C, F, H**).

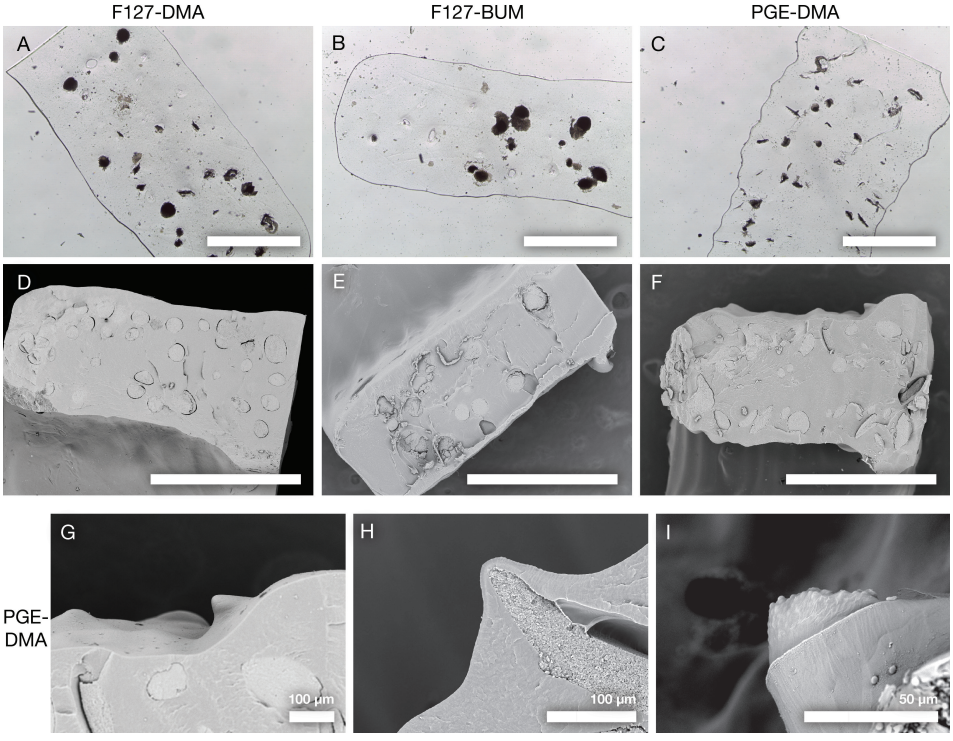

Figure 15. Optical microscopy (OM) and scanning electron microscopy (SEM) micrographs of engineered living materials (ELMs) after 48 h of incubation (A − F) and the escape mode of cells from PGE-DMA (G − I). Peripheral colonies in PGE-DMA formed spindlelike structures (C, F, H), while F127-DMA and F127-BUM formed spherical colonies (A, B, D, E). When the material broke, cells began to escape into the medium (I). Scale bar is 1 mm unless marked differently [I].

5.4.4. Mechanical properties of micellar hydrogels and their relevance to cell retention

As a spherical cell colony expands within a hydrogel, it induces both compressive and tensile stress on the surrounding hydrogel matrix. The primary mechanism is radial expansion, where an increase in colony volume exerts outward forces on the polymer matrix. In resisting deformation, the hydrogel undergoes elastic stretching, producing tensile stress in the bulk while simultaneously experiencing compression at the colony–matrix interface. Hardness itself is not a fundamental material parameter but rather a response to the superposition of these stresses. Shore hardness testing, which involves indentation with a tip, provides a practical proxy for this behaviour by capturing the material's overall resistance to deformation — an analogue to the stresses exerted by an expanding colony within the matrix.

To evaluate the relevance of such cell-generated mechanical stresses in ELM systems, pre-swollen hydrogel samples were tested in a PBS water bath at the lowest available crosshead speed, trying to simulate the gradual deformation caused by cell proliferation. The tensile stress–strain profiles of F127-DMA, F127-BUM, and PGE-DMA hydrogels are shown in **Figure 16A**. F127-BUM (30 wt%) exhibited the highest tensile strength at 0.31 ± 0.02 MPa, whereas PGE-DMA (20 wt%) reached only 0.15 ± 0.01 MPa. The latter was expected due to the reverse micellar polymer network shielding functional groups within the micelle core, reducing the likelihood of micelle-micelle cross-polymerisation. F127-DMA demonstrated the highest stretchability (97 ± 11%), a property likely linked to its lower functionalisation degree, which permits greater chain mobility and elongation under stress. A comparable level of stretchability was observed for F127-BUM at 20% w/w (88 ± 1%), likely due to fewer chain entanglements at lower polymer concentrations, which permit greater extension before rupture.

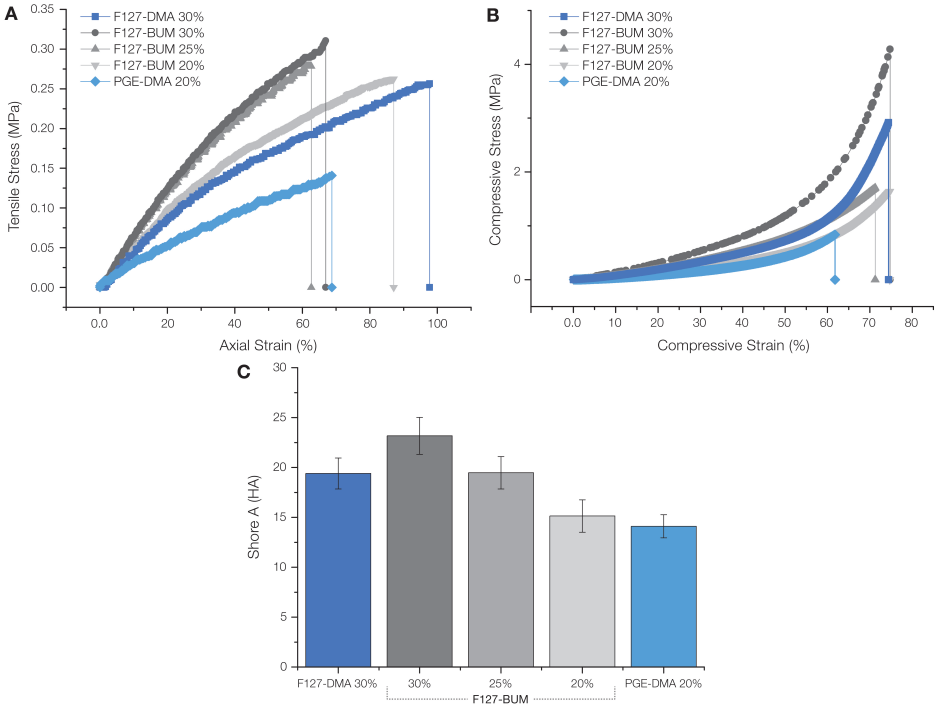

Figure 16. Tensile (A) and compression (B) measurement results for all 3D-printed hydrogels after 24 hours of stabilisation in PBS. Shore A hardness (C) of the tested hydrogels [IV].

The overall toughness values (**Table 3**) correlate with cell retention data in ELM experiments highlighted in Section 5.4.2. These findings indicate that the toughness of hydrogels corresponds to longer retention times in ELMs rather than their underlying storage modulus.

Table 3. The mechanical properties of the printed hydrogels after swelling (24 h) at 24 ± 1 °C in 0.1M PBS [IV].

Polymer	% w/w	E_σ (MPa)	Max σ (MPa)	σ Strain (%)	Toughness ($kJ \cdot m^{-3}$)	$E_{\sigma c}$ (MPa)	Max σ_c (MPa)	σ_c Strain (%)
F127-DMA	30%	0.47 ± 0.01	0.26 ± 0.02	97 ± 11	150 ± 25	0.79 ± 0.06	2.9 ± 0.2	74.5 ± 0.4
F127-BUM	30%	0.71 ± 0.02	0.31 ± 0.02	67 ± 6	119 ± 20	1.36 ± 0.02	4.1 ± 0.2	74.2 ± 0.6
	25%	0.63 ± 0.03	0.27 ± 0.05	60 ± 12	96 ± 38	0.84 ± 0.02	1.7 ± 0.3	71.2 ± 3.3
	20%	0.48 ± 0.02	0.26 ± 0.01	88 ± 1	133 ± 5	0.63 ± 0.01	1.6 ± 0.4	74.0 ± 4.5
PGE-DMA	20%	0.23 ± 0.01	0.15 ± 0.01	69 ± 2	55 ± 6	0.37 ± 0.01	0.83 ± 0.01	61.7 ± 0.6

Compression tests (**Figure 16B**) further substantiated these trends. Similar to tensile behaviour, PGE-DMA displayed the lowest deformation tolerance, fracturing at ~60% strain with a compressive strength of 0.83 ± 0.01 MPa. F127-based hydrogels with higher polymer concentrations showed greater compressive strength, confirming the contribution of crosslink density to bulk deformation resistance.

Shore A hardness measurements (**Figure 16C**) aligned closely with tensile and compression data. While Shore hardness and Young's modulus relationships are well established for elastomeric materials [132–134], their use as a rapid screening metric in the context of ELMs has, to our knowledge, not been reported. These findings suggest that simple Shore hardness testing can serve as a rapid and reliable proxy for hydrogel mechanics, providing a valuable initial approximation of how the matrix may influence cell morphology, growth, and retention in ELMs.

5.4.4.1. *In Silico* modelling of cellular expansion and matrix failure

To investigate the microscale mechanical interplay between expanding cell colonies and the surrounding hydrogel, yeast colony growth in 30 wt% F127-BUM was simulated in COMSOL Multiphysics. The matrix was parametrised using tensile data from 3D-printed samples of 30 wt% F127-BUM (Section 5.4.4; **Figure 17A**).

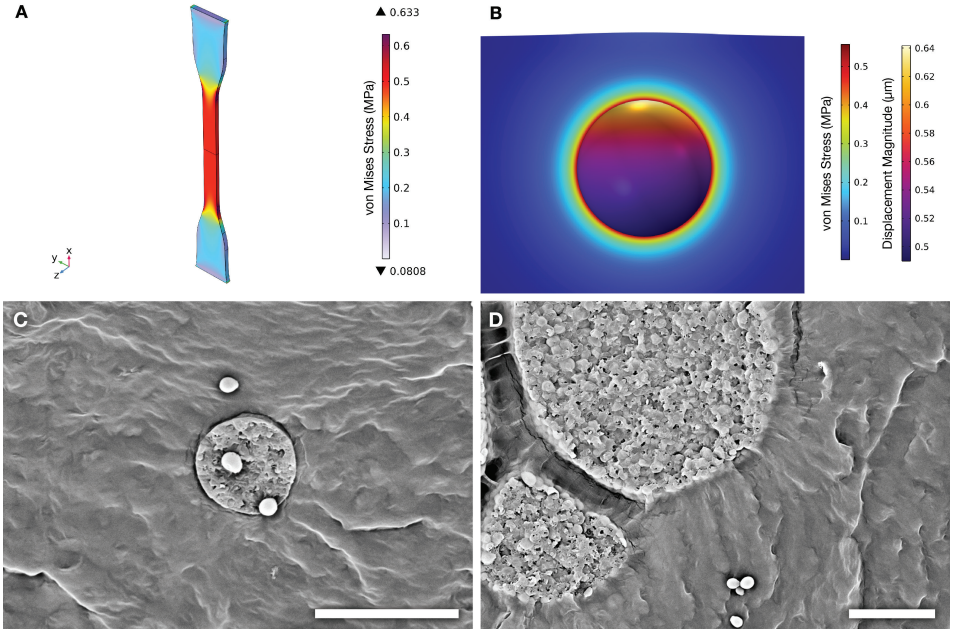

Figure 17. (A) *In silico* tensile test reconstruction and stress distribution in a sample at maximum deformation; (B) *In silico* simulated stresses caused by colony expansion in swollen 30% F127-BUM; (C, D) SEM micrograph of a cell colony embedded in 30% F127-BUM hydrogel with an initial cell loading density of 10^6 cells per gram of hydrogel (scale bar 20 µm) [IV].

F127-BUM was selected because it was fully functionalised and exhibited the highest tensile strength of the tested hydrogels. To isolate and investigate the material's fundamental limiting factors and mechanical response under localised stress — without interference from neighbouring colonies — the final model considered a single yeast colony positioned near the construct surface. The simulation revealed high local von Mises stress concentrations at the cell-matrix interface (**Figure 17B**), with local stresses approaching the experimentally measured tensile strength once the colony diameter reached ~10 µm. These computational findings align well with SEM imaging of the corresponding ELMs (**Figure 17C, D**), which reveal radial microfractures and localised matrix deformation patterns that increase with increasing colony size, closely matching the simulated stress distributions. Together, these results suggest that matrix rupture occurs through a progressive mechanical compromise driven by local stress accumulation around growing colonies, rather than an abrupt failure. Increasing network toughness and its capacity to dissipate stress, therefore, appears critical for extending ELM longevity and bioproduction reliability. Linking bulk mechanical testing, simulation, and microscale imaging establishes a predictive framework for guiding the design of next-generation biofunctional materials.

5.5. Long-term stability and material limitations

On the surface, the BUM derivative of F127 appears to be a more favourable choice for creating ELMs due to its higher functionalisation percentage and superior mechanical properties. However, the stability of the amide bond is a concern, as it is potentially susceptible to cell-secreted peptidases [I]. A time-related issue was also identified, as the tensile strength and overall toughness of F127-BUM decreased by nearly 50% after one month of storage in PBS at room temperature. Meanwhile, the strain-at-break remained essentially unchanged, a trend not observed with F127-DMA over the same period. The underlying reasons remain unclear, as both polymers contain ester bonds in their functional groups, and in theory, the amide bond in F127-BUM should exhibit greater stability against hydrolytic and oxidative degradation. A possible explanation could be the differences in interactions with the surrounding aqueous environment, as the amide group may enhance the region's hydrophilicity and potentially accelerate the degradation [135–137]. Further research is required to explore the stability and degradation mechanisms of F127-BUM. While these limitations do not impact short-term experiments or applications where controlled degradation is beneficial, they are crucial for long-term studies and industrial ELM applications.

5.6. Polymer-cell interactions: thin-film formation

A particularly striking observation was the presence of a thin organic coating surrounding colonies in F127-based hydrogels, which was absent in PGE-DMA hydrogels (**Figures 18A–C**). This thin film likely formed due to the distinct

micellar identity of these polymers, which enabled specific interactions with the hydrophilic yeast cell wall. These interactions altered micelle alignment and the positioning of polymerisable groups around the cells prior to photo-crosslinking. Molecular dynamics simulations have shown that the PEO blocks of long-chain poloxamers adsorb onto the hydrophilic surface of the lipid bilayer, while the PPO regions orient outwards [138]. The yeast cell wall is even more hydrophilic than the membrane due to its polysaccharide-rich composition, which further promotes the adsorption and alignment of block copolymers. A supercritical CO_2 extraction protocol, involving the rapid release of CO_2, was used to separate and measure the thin polymer coating (100–160 nm in unhydrated form) surrounding yeast colonies (**Figure A3**). As colonies expanded beyond ~60–80 µm, this polymer film ruptured, and only remnants of the coating were observed on a colony surface (**Figure A4**).

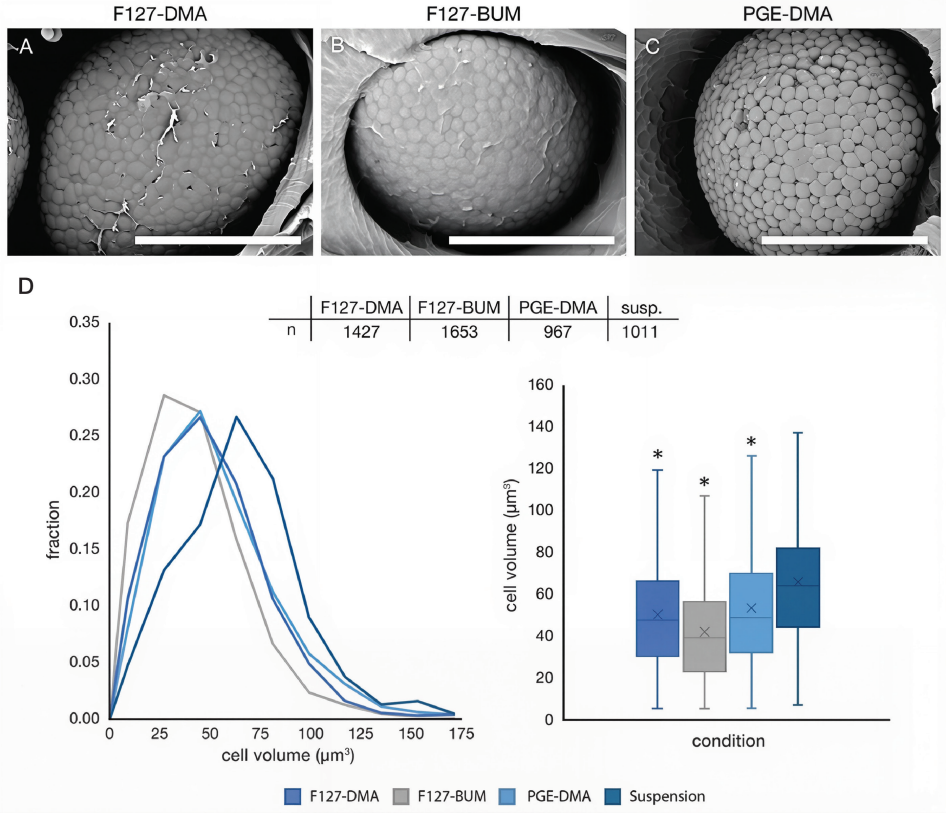

Figure 18. Organic film covers yeast cell colonies in ELMs and cell volume (µm^3). F127-DMA (A) and F127-BUM (B) both had a thin organic coating around colonies, while PGE-DMA (C) lacked a similar polymer coating. Scale bar is 30 µm. Cell volume (in µm^3) distribution in ELMs and suspension cell culture (D). A total of ≥ 967 cells per condition were analysed. ELMs were incubated for 48 h before processing and measurement. *$p < 0.05$, significant difference from suspension cells, x: mean [I].

5.7. Phenotypic impact of physical confinement

The variations in cell–polymer interactions and retention times consequently raised the question of how physical confinement influences cell phenotype. We performed a computational analysis on the acquired SEM images to address this question. During this analysis, the cell size (volume in μm^3) parameter was utilised to investigate the effects of physical confinement on the cells in hydrogels in comparison to suspension cells. Interestingly, cells encapsulated in hydrogels were significantly ($p < 0.05$) smaller than the suspension cells. Cell size differences were even evident among the ELMs (Figures 18D, C). The observed differences in cell size are likely the result of multiple contributing factors rather than a single cause, since cellular phenotype represents the integrated outcome of numerous processes [139,140]. In addition, physical confinement within hydrogels introduces further constraints that do not apply to cells in suspension. Nevertheless, data suggest that a higher storage modulus leads to a smaller cell size.

5.8. Diffusion constraints and metabolic control in ELMs

The bioproduction performance of ELMs is fundamentally determined by the transport of nutrients, gases, and metabolites through the encapsulating hydrogel matrix. The following section demonstrates that physical confinement and restricted diffusion in ELMs based on micellar hydrogels alter microbial physiology, shifting metabolism toward fermentation and opening possibilities for designing oxygen-restricted bioprocesses.

5.8.1. Substrate and product diffusion and ELM metabolic activity

To establish a baseline for small-molecule transport, the diffusion coefficients of glucose and EtOH were measured in 30% F127 DMA abiotic hydrogels within a PBS environment. PBS was chosen because it closely mimics the ionic strength and osmolarity of a wide range of cell culture media, ensuring the results are broadly applicable across different microbial taxa and not limited to a single organism or kingdom.

In the hydrogel, glucose and EtOH diffusion are 3.6 ± 1.1 and 2.5 ± 0.3 times slower than in water [141] (**Figure 19**). Unlike the linear temperature dependence observed in aqueous systems [141], a distinct diffusion peak occurred near 20 °C in the hydrogel, coinciding with the UV-curing and gelation temperature. This behaviour may reflect a micelle organisation “memory” effect induced by micelle formation and UV-curing at this temperature range. However, further research is required to comprehend the underlying causes of this phenomenon.

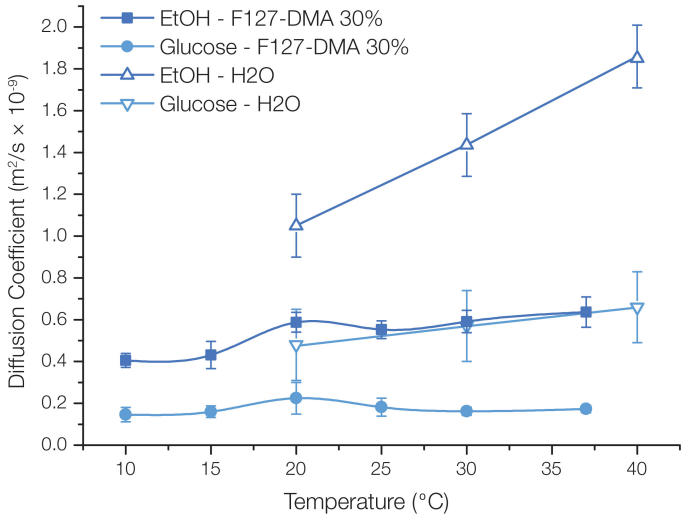

Figure 19. Diffusion coefficients of ethanol (EtOH) and glucose in 30% F127 DMA, compared to their diffusion coefficients in water [141], offer valuable insights into the transport properties of these substances within the micellar hydrogel [IV].

In the context of bioproduction, the observed diffusional delay for glucose aligns well with the extended glucose phase observed in biologically active F127-BUM ELMs, which lasted over 40 h — approximately 2.5 times longer than in suspension cultures (**Figure 20**). The 3.6 ± 1.1 fold reduction in glucose diffusion within F127-based hydrogels (relative to water) suggests that substrate supply may represent the primary bottleneck under conditions of high metabolic demand. In addition, EtOH accumulation caused by its 2.5 ± 0.3 fold slower diffusion could further contribute to metabolic inhibition, particularly during prolonged cultivation. Despite the extended glucose-consumption phase, EtOH yield from glucose was 13.6% higher in ELMs than in suspension culture (SC) (**Figure 20**).

Given its relatively small molecule, the diffusional behaviour observed for glucose suggests that larger molecular species are likely to encounter even greater restrictions in such gels, particularly at elevated temperatures; the underlying reasons for this are discussed in Section 5.1.3.

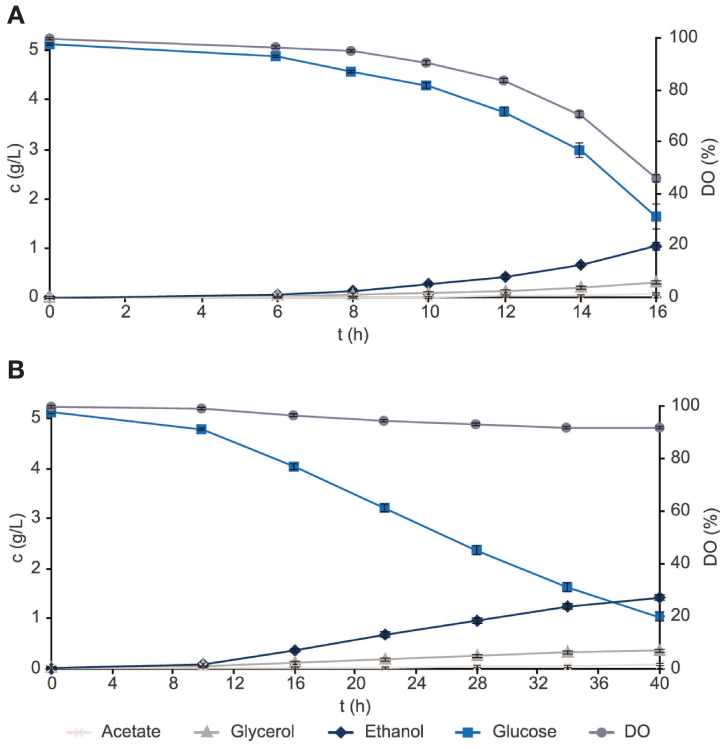

Figure 20. Yeast physiology in the glucose phase of batch cultivation. (A) Suspension cells; (B) 30% F127-BUM ELMs. Key: DO — dissolved oxygen. Error bars represent standard deviations, n = 3 [III].

5.8.2. Oxygen exclusion and microaerobic shift

Dissolved oxygen measurements revealed that yeast in F127-BUM ELMs experienced almost complete respiratory suppression during glucose metabolism (**Figure 20B**). In these constructs, yeast consumed glucose primarily through fermentation because the mitochondrial respiratory chain, which depends on oxygen as the terminal electron acceptor under aerobic conditions, had no access to oxygen. Whereas suspension cultures consumed glucose exponentially and depleted oxygen within 16 h, the ELMs showed linear glucose uptake with negligible oxygen utilisation.

To verify that oxygen restriction was matrix-induced rather than a result of physiological adaptation, pre-cultured cells and ELM were transferred to EtOH-containing medium, where oxygen is essential for EtOH metabolism. While suspension culture consumed EtOH and produced biomass, ELM failed to grow under these conditions. This confirmed the effective anoxia within the hydrogel network (**Figure 21**). Physiological changes in the ELMs during the EtOH phase included increased vacuolisation, reduced cell dry weight, and decreased viability (93.5%), all consistent with responses to environmental stress [142,143].

These observations indicate that F127-BUM hydrogels are highly restrictive for oxygen transport, to the extent that mitochondrial respiration is completely suppressed. As such, the oxygen-impermeability of F127-BUM hydrogels could be strategically exploited to create microaerobic or anoxic compartments in multikingdom constructs, or to cultivate obligate anaerobes without complex bioreactor control systems. Nevertheless, an in-depth investigation of oxygen diffusion in micellar hydrogels could clarify the underlying causes of the pronounced anoxia. Given that these hydrogels contain more than 75% water in the swollen state (Section 5.1.2), such a substantial limitation on oxygen transport is somewhat unexpected and may be linked to polymer interactions and their orientation around cells, including the thin film formation described in Section 5.6.

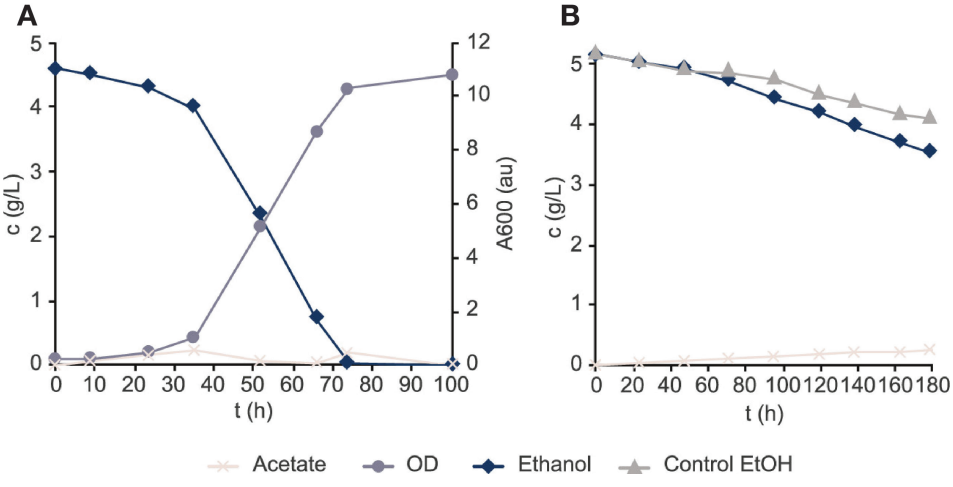

Figure 21. Evaluation of the respiratory metabolism using a defined medium with ethanol (EtOH) as the carbon source. (A) Suspension cells; (B) 30% F127-BUM ELM. Key: OD-optical density. N = 1 [III].

5.8.3. ELM-based beer brewing: enhanced EtOH production

To assess the translational potential of these findings — higher EtOH yields on glucose and minimal respiration — a scaled-up fermentation platform was designed using ELMs loaded with the brewer's yeast strain Bry-97, cultivated in a standard wort formulation for a pale ale-style beer. Compared with conventional suspension brewing, the 3D-printed constructs produced 3.73% more EtOH after 14 days under identical conditions. Although cell leakage began around day five, the printed constructs outperformed batch cultures in EtOH conversion efficiency and final product clarity (**Figure 22**). Beer colour measurements also showed differences, with SC beer appearing darker. Sensory evaluation indicated that ELM-brewed beer had a lighter taste, with sweeter notes and less pronounced yeast flavour compared with SC beer. Both beers were equally well-carbonated.

These results provide a promising foundation for developing cost-effective, sustainable, and reusable fermentation platforms applicable to brewing and on-demand biochemical production. Future advances in materials and fabrication processes are expected to provide further advantages, including removing the post-fermentation filtration step and cost savings from reduced substrate requirements to reach equivalent alcohol levels as in conventional systems.

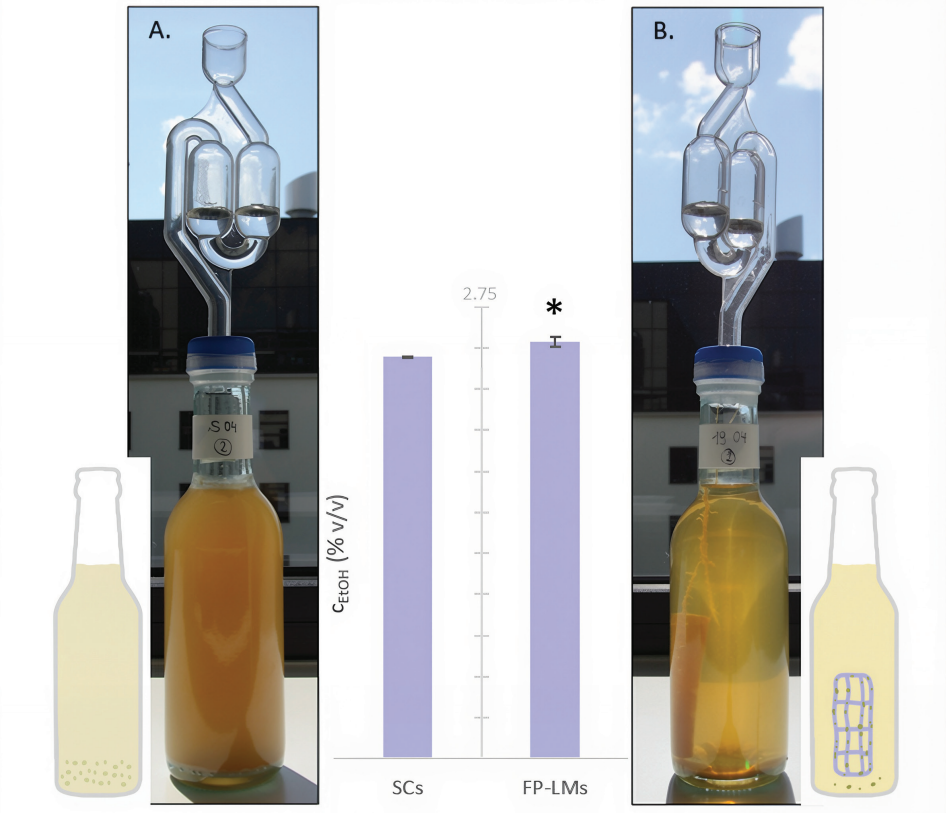

Figure 22: (A) Bottle fermentation of beer with suspension cultures (SCs) and (B) engineered living materials (ELMs). Alcohol content measured after 14 days. *$p < 0.05$ (one tail), significant difference from SCs; $n = 2$, each. Y-axis partitioning: 0.25% [III].

6. CONCLUSIONS

This thesis investigated how photo-crosslinkable micellar hydrogels — specifically F127-BUM, F127-DMA and PGE-DMA — can be applied as structural and functional matrices for 3D-printed ELMs. The work focused on how micellar hydrogels govern spatial organisation, cell proliferation, phenotype and metabolism, with the broader aim of identifying design rules for scalable, spatially organised and metabolically programmable living systems.

First, the printability and structural fidelity of these materials were examined. Consistent with previous reports, all tested hydrogels can be extruded, photopolymerised, and formed into well-defined 3D constructs with complex geometries. Distinct microbial populations (bacteria, yeast, algae) were co-printed into separate compartments within the same construct, maintaining clear interfaces and only minimal cross-bleeding, confirming that micellar hydrogels can support spatially resolved, multi-kingdom assemblies. At the same time, these materials displayed considerable post-printing swelling and thermo-responsive changes in water content and hardness. Thus, the final geometry and mechanical behaviour are governed not only by the printing step itself but also by post-printing equilibration, which must be factored into the design.

Acellular controls demonstrated that crosslinked hydrogels remained structurally stable in cultivation media, without creep, mass loss or observable degradation. This established a baseline against which biological effects — such as cell-induced deformation, swelling, and mass increase — can be attributed to cell activity rather than underlying material properties.

The biological performance of these systems was examined. F127-BUM hydrogel matrix supported high viability (>90%) of yeast, bacteria and algae. Cells remained confined to their printed regions within the construct, with occasional leakage into the surrounding medium from peripheral cells. This indicates that the hydrogel network functions as a selective barrier, permitting nutrient transport while restricting cellular migration. Such behaviour enables the co-localisation of different microorganisms in close proximity without uncontrolled invasion.

Growth analysis revealed that the encapsulated yeast did not proliferate uniformly. Colonies near the periphery expanded more rapidly and reached larger diameters than those deeper in the construct, where diffusion-limited nutrient availability was lower. Importantly, different hydrogels imposed distinct spatial growth modes: F127-based systems promoted circular colony growth formation, whereas PGE-DMA supported more irregular spindle-like growth. These results show that hydrogel chemistry and architecture shape local “ecologies” within the material. They also indicate that simply printing thicker constructs does not directly translate to proportionally higher productive biomass, because mass transport becomes limiting.

Cell retention and construct durability were found to depend on mechanical behaviour. Retention time differed between materials and correlated with toughness and fracture resistance rather than bulk stiffness alone. Mechanical testing

and modelling demonstrated that expanding colonies generate local stress concentrations that eventually exceed the failure threshold of the matrix. Cell leakage is therefore primarily a mechanical failure rather than a biological one: cells escape when local stresses cause cracks, microfractures, or ruptures in the hydrogel matrix. Extending ELM`s lifespan will therefore depend on improving the material's ability to resist fracture and dissipate stress, not simply on increasing its stiffness (modulus).

Diffusion studies showed that glucose and EtOH diffusion are substantially slower through the F127-based hydrogel compared to water, and metabolic studies revealed that oxygen transport into the encapsulated regions is strongly limited. As a result, yeast in F127-BUM adopted and maintained a predominantly fermentative metabolism, even in conditions where planktonic cultures of the same strain were respiratory. In this way, the hydrogel matrix itself constrains the metabolic state via physical confinement and oxygen limitation, without any genetic intervention or external aeration control.

Ultimately, these principles were demonstrated in a practical context. 3D-printed constructs loaded with brewing yeast produced higher EtOH yield and clearer final product than equivalent suspension cultures under identical conditions. This confirms that micellar hydrogel-based ELMs can act as metabolically tuned biocatalytic units.

In summary, this work shows that micellar hydrogels are not passive supports but active regulators of spatial patterning, mechanical containment, cellular retention, and metabolism. The results establish practical design relationships linking printability, mechanical behaviour, and diffusional transport to biological function, thereby enabling more robust, compartmentalised, and programmable ELMs for future bioprocesses.

REFERENCES

[1] P. Stegmann, M. Londo, M. Junginger, The circular bioeconomy: Its elements and role in European bioeconomy clusters, Resources, Conservation & Recycling: X 6 (2020) 100029. https://doi.org/10.1016/J.RCRX.2019.100029.

[2] M.M. Bugge, T. Hansen, A. Klitkou, What Is the Bioeconomy? A Review of the Literature, Sustainability 2016, Vol. 8, Page 691 8 (2016) 691. https://doi.org/10.3390/SU8070691.

[3] J. Philp, D. Winickoff, Realising the circular bioeconomy, OECD Science, Technology and Industry Policy Papers (2018). https://doi.org/10.1787/31bb2345-en.

[4] R. Kamusoko, R.M. Jingura, W. Parawira, Z. Chikwambi, Strategies for valorization of crop residues into biofuels and other value-added products, Biofuels, Bioproducts and Biorefining 15 (2021) 1950–1964. https://doi.org/10.1002/BBB.2282.

[5] Y.F. Tsang, V. Kumar, P. Samadar, Y. Yang, J. Lee, Y.S. Ok, H. Song, K.H. Kim, E.E. Kwon, Y.J. Jeon, Production of bioplastic through food waste valorization, Environ Int 127 (2019) 625–644. https://doi.org/10.1016/J.ENVINT.2019.03.076.

[6] C.G. Otoni, H.M.C. Azeredo, B.D. Mattos, M. Beaumont, D.S. Correa, O.J. Rojas, The Food–Materials Nexus: Next Generation Bioplastics and Advanced Materials from Agri-Food Residues, Advanced Materials 33 (2021) 2102520. https://doi.org/10.1002/ADMA.202102520.

[7] K.C. Obileke, H. Onyeaka, E.L. Meyer, N. Nwokolo, Microbial fuel cells, a renewable energy technology for bio-electricity generation: A mini-review, Electrochem Commun 125 (2021) 107003. https://doi.org/10.1016/J.ELECOM.2021.107003.

[8] S. Malik, S. Kishore, A. Dhasmana, P. Kumari, T. Mitra, V. Chaudhary, R. Kumari, J. Bora, A. Ranjan, T. Minkina, V.D. Rajput, A Perspective Review on Microbial Fuel Cells in Treatment and Product Recovery from Wastewater, Water 2023, Vol. 15, Page 316 15 (2023) 316. https://doi.org/10.3390/W15020316.

[9] A.M. Henstra, J. Sipma, A. Rinzema, A.J. Stams, Microbiology of synthesis gas fermentation for biofuel production, Curr Opin Biotechnol 18 (2007) 200–206. https://doi.org/10.1016/J.COPBIO.2007.03.008.

[10] F.M. Liew, M.E. Martin, R.C. Tappel, B.D. Heijstra, C. Mihalcea, M. Köpke, Gas Fermentation-A flexible platform for commercial scale production of low-carbon-fuels and chemicals from waste and renewable feedstocks, Front Microbiol 7 (2016) 202812. https://doi.org/10.3389/FMICB.2016.00694.

[11] M. Pavan, K. Reinmets, S. Garg, A.P. Mueller, E. Marcellin, M. Köpke, K. Valgepea, Advances in systems metabolic engineering of autotrophic carbon oxide-fixing biocatalysts towards a circular economy, Metab Eng 71 (2022) 117–141. https://doi.org/10.1016/J.YMBEN.2022.01.015.

[12] B.K. Adhikari, S. Barrington, J. Martinez, Predicted growth of world urban food waste and methane production, Waste Management & Research 24 (2006) 421–433. https://doi.org/10.1177/0734242X06067767.

[13] J.M. Clomburg, A.M. Crumbley, R. Gonzalez, Industrial biomanufacturing: The future of chemical production, Science (1979) 355 (2017). https://doi.org/10.1126/science.aag0804.

[14] J.S. Yuan, M.J. Pavlovich, A.J. Ragauskas, B. Han, Biotechnology for a sustainable future: biomass and beyond, Trends Biotechnol 40 (2022) 1395–1398. https://doi.org/10.1016/j.tibtech.2022.09.020.

[15] C.J. Franzén, L. Olsson, K.S. Johansen, The lignocellulosic biorefinery concept is sound: a commentary on Zhao et al., Trends Biotechnol 42 (2024) 395–396. https://doi.org/10.1016/J.TIBTECH.2023.12.005.
[16] R. Takors, Food for Thoughts for Prospective Biomanufacturing, Microb Biotechnol 18 (2025) e70088. https://doi.org/10.1111/1751-7915.70088.
[17] D. Voet, J.G. Voet, Biochemistry, 4th Edition | Wiley, Wiley (2010) 1520. https://www.wiley.com/en-us/Biochemistry%2C+4th+Edition-p-9780470570951 (accessed October 10, 2025).
[18] F. Verdú-Navarro, J.A. Moreno-Cid, J. Weiss, M. Egea-Cortines, The advent of plant cells in bioreactors, Front Plant Sci 14 (2023) 1310405. https://doi.org/10.3389/FPLS.2023.1310405.
[19] J.D. Yang, C. Lu, B. Stasny, J. Henley, W. Guinto, C. Gonzalez, J. Gleason, M. Fung, B. Collopy, M. Benjamino, J. Gangi, M. Hanson, E. Ille, Fed-batch bioreactor process scale-up from 3-L to 2,500-L scale for monoclonal antibody production from cell culture, Biotechnol Bioeng 98 (2007) 141–154. https://doi.org/10.1002/BIT.21413.
[20] T. Zinnecker, U. Reichl, Y. Genzel, Innovations in cell culture-based influenza vaccine manufacturing–from static cultures to high cell density cultivations, Hum Vaccin Immunother 20 (2024). https://doi.org/10.1080/21645515.2024.2373521.
[21] M.T. de Pinho Favaro, J. Atienza-Garriga, C. Martínez-Torró, E. Parladé, E. Vázquez, J.L. Corchero, N. Ferrer-Miralles, A. Villaverde, Recombinant vaccines in 2022: a perspective from the cell factory, Microb Cell Fact 21 (2022) 1–17. https://doi.org/10.1186/S12934-022-01929-8.
[22] K.P. Jayapal, K.F. Wlaschin, W.S. Hu, M.G.S. Yap, Recombinant protein therapeutics from CHO Cells – 20 years and counting, Chem Eng Prog 103 (2007) 40–47. https://experts.umn.edu/en/publications/recombinant-protein-therapeutics-from-cho-cells-20-years-and-coun (accessed October 10, 2025).
[23] N.A. Baeshen, M.N. Baeshen, A. Sheikh, R.S. Bora, M.M.M. Ahmed, H.A.I. Ramadan, K.S. Saini, E.M. Redwan, Cell factories for insulin production, Microb Cell Fact 13 (2014) 1–9. https://doi.org/10.1186/S12934-014-0141-0/TABLES/3.
[24] J. Yadav, H. Marwah, C. Kumar, Synthetic biology and metabolic engineering paving the way for sustainable next-gen biofuels: a comprehensive review, Energy Advances 4 (2025) 1209–1228. https://doi.org/10.1039/D5YA00118H.
[25] S. Shi, Z. Wang, L. Shen, H. Xiao, Synthetic biology: a new frontier in food production, Trends Biotechnol 40 (2022) 781–803. https://doi.org/10.1016/J.TIBTECH.2022.01.002.
[26] S.M. Mirsalami, M. Mirsalami, Advances in genetically engineered microorganisms: Transforming food production through precision fermentation and synthetic biology, Future Foods 11 (2025) 100601. https://doi.org/10.1016/J.FUFO.2025.100601.
[27] C.A. Voigt, Synthetic biology 2020–2030: six commercially-available products that are changing our world, Nat Commun 11 (2020) 1–6. https://doi.org/10.1038/S41467-020-20122-2.
[28] A. Kubis, A. Bar-Even, Synthetic biology approaches for improving photosynthesis, J Exp Bot 70 (2019) 1425–1433. https://doi.org/10.1093/JXB/ERZ029.
[29] M.I.S. Naduthodi, N.J. Claassens, S. D'Adamo, J. van der Oost, M.J. Barbosa, Synthetic Biology Approaches To Enhance Microalgal Productivity, Trends Biotechnol 39 (2021) 1019–1036. https://doi.org/10.1016/J.TIBTECH.2020.12.010.

[30] P. Van Nies, I. Westerlaken, D. Blanken, M. Salas, M. Mencía, C. Danelon, Self-replication of DNA by its encoded proteins in liposome-based synthetic cells, Nat Commun 9 (2018) 1–12. https://doi.org/10.1038/S41467-018-03926-1.
[31] A. Samanta, L. Baranda Pellejero, M. Masukawa, A. Walther, DNA-empowered synthetic cells as minimalistic life forms, Nat Rev Chem 8 (2024) 454–470. https://doi.org/10.1038/S41570-024-00606-1.
[32] P. Rugbjerg, M.O.A. Sommer, Overcoming genetic heterogeneity in industrial fermentations, Nat Biotechnol 37 (2019) 869–876. https://doi.org/10.1038/S41587-019-0171-6.
[33] J. Nielsen, J.D. Keasling, Engineering Cellular Metabolism, Cell 164 (2016) 1185–1197. https://doi.org/10.1016/J.CELL.2016.02.004.
[34] S. Van Dien, From the first drop to the first truckload: commercialization of microbial processes for renewable chemicals, Curr Opin Biotechnol 24 (2013) 1061–1068. https://doi.org/10.1016/J.COPBIO.2013.03.002.
[35] S.Y. Lee, H.U. Kim, Systems strategies for developing industrial microbial strains, Nat Biotechnol 33 (2015). https://doi.org/10.1038/nbt.3365.
[36] F. Wang, W. Zhang, Synthetic biology: Recent progress, biosafety and biosecurity concerns, and possible solutions, J Biosaf Biosecur 1 (2019) 22–30. https://doi.org/10.1016/J.JOBB.2018.12.003.
[37] J. Li, H. Zhao, L. Zheng, W. An, Advances in Synthetic Biology and Biosafety Governance, Front Bioeng Biotechnol 9 (2021) 598087. https://doi.org/10.3389/FBIOE.2021.598087.
[38] M. Braun, S. Fernau, P. Dabrock, M. Braun, S. Fernau, P. Dabrock, (Re-) Designing Nature? An Overview and Outlook on the Ethical and Societal Challenges in Synthetic Biology, Adv Biosyst 3 (2019) 1800326. https://doi.org/10.1002/ADBI.201800326.
[39] H. Torgersen, Synthetic biology in society: Learning from past experience?, Syst Synth Biol 3 (2009) 9–17. https://doi.org/10.1007/S11693-009-9030-Y.
[40] P.Q. Nguyen, N.M.D. Courchesne, A. Duraj-Thatte, P. Praveschotinunt, N.S. Joshi, Engineered Living Materials: Prospects and Challenges for Using Biological Systems to Direct the Assembly of Smart Materials, Advanced Materials 30 (2018) 1–34. https://doi.org/10.1002/adma.201704847.
[41] D. Wangpraseurt, S. You, Y. Sun, S. Chen, Biomimetic 3D living materials powered by microorganisms, Trends Biotechnol 40 (2022) 843–857. https://doi.org/10.1016/j.tibtech.2022.01.003.
[42] A. Rodrigo-Navarro, S. Sankaran, M.J. Dalby, A. del Campo, M. Salmeron-Sanchez, Engineered living biomaterials, Nat Rev Mater 6 (2021) 1175–1190. https://doi.org/10.1038/s41578-021-00350-8.
[43] W. V. Srubar, The defining moment for engineered living materials, Matter 5 (2022) 2556–2557. https://doi.org/10.1016/j.matt.2022.07.006.
[44] A.D. Lantada, J.G. Korvink, M. Islam, Taxonomy for engineered living materials, Cell Rep Phys Sci 3 (2022). https://doi.org/10.1016/j.xcrp.2022.100807.
[45] S. Molinari, R.F. Tesoriero, C.M. Ajo-Franklin, Bottom-up approaches to engineered living materials: Challenges and future directions, Matter 4 (2021) 3095–3120. https://doi.org/10.1016/J.MATT.2021.08.001.

[46] C. Gilbert, T. Ellis, Biological Engineered Living Materials: Growing Functional Materials with Genetically Programmable Properties, ACS Synth Biol 8 (2018) 1–15. https://doi.org/10.1021/ACSSYNBIO.8B00423.
[47] U.O.S. Seker, A.Y. Chen, R.J. Citorik, T.K. Lu, Synthetic Biogenesis of Bacterial Amyloid Nanomaterials with Tunable Inorganic–Organic Interfaces and Electrical Conductivity, ACS Synth Biol 6 (2016) 266–275. https://doi.org/10.1021/ACSSYNBIO.6B00166.
[48] P.Q. Nguyen, Z. Botyanszki, P.K.R. Tay, N.S. Joshi, Programmable biofilm-based materials from engineered curli nanofibres, Nature Communications 2014 5:1 5 (2014) 4945-. https://doi.org/10.1038/ncomms5945.
[49] S.Y. Kang, A. Pokhrel, S. Bratsch, J.J. Benson, S.O. Seo, M.B. Quin, A. Aksan, C. Schmidt-Dannert, Engineering Bacillus subtilis for the formation of a durable living biocomposite material, Nature Communications 2021 12:1 12 (2021) 7133- https://doi.org/10.1038/s41467-021-27467-2.
[50] L. Liang, C. Heveran, R. Liu, R.T. Gill, A. Nagarajan, J. Cameron, M. Hubler, W. V. Srubar, S.M. Cook, Rational Control of Calcium Carbonate Precipitation by Engineered Escherichia coli, ACS Synth Biol 7 (2018) 2497–2506. https://doi.org/10.1021/ACSSYNBIO.8B00194.
[51] C.M. Heveran, S.L. Williams, J. Qiu, J. Artier, M.H. Hubler, S.M. Cook, J.C. Cameron, W. V. Srubar, Biomineralization and Successive Regeneration of Engineered Living Building Materials, Matter 2 (2020) 481–494. https://doi.org/10.1016/J.MATT.2019.11.016.
[52] W. V. Srubar, Engineered Living Materials: Taxonomies and Emerging Trends, Trends Biotechnol 39 (2021) 574–583. https://doi.org/10.1016/j.tibtech.2020.10.009.
[53] X. Liu, T.C. Tang, E. Tham, H. Yuk, S. Lin, T.K. Lu, X. Zhao, Stretchable living materials and devices with hydrogel-elastomer hybrids hosting programmed cells, Proc Natl Acad Sci U S A 114 (2017) 2200–2205. https://doi.org/10.1073/PNAS.1618307114.
[54] P. Praveschotinunt, A.M. Duraj-Thatte, I. Gelfat, F. Bahl, D.B. Chou, N.S. Joshi, Engineered E. coli Nissle 1917 for the delivery of matrix-tethered therapeutic domains to the gut, Nature Communications 2019 10:1 10 (2019) 5580-. https://doi.org/10.1038/s41467-019-13336-6.
[55] S. Sankaran, J. Becker, C. Wittmann, A. Del Campo, S. Sankaran, A. Del Campo, J. Becker, C. Wittmann, Optoregulated Drug Release from an Engineered Living Material: Self-Replenishing Drug Depots for Long-Term, Light-Regulated Delivery, Small 15 (2019) 1804717. https://doi.org/10.1002/SMLL.201804717.
[56] I. Jung, H. Bin Seo, J. eun Lee, B. Chan Kim, M.B. Gu, A dip-stick type biosensor using bioluminescent bacteria encapsulated in color-coded alginate microbeads for detection of water toxicity, Analyst 139 (2014) 4696–4701. https://doi.org/10.1039/C4AN00308J.
[57] P.K.R. Tay, P.Q. Nguyen, N.S. Joshi, A Synthetic Circuit for Mercury Bioremediation Using Self-Assembling Functional Amyloids, ACS Synth Biol 6 (2017) 1841–1850. https://doi.org/10.1021/ACSSYNBIO.7B00137.
[58] W. De Muynck, N. De Belie, W. Verstraete, Microbial carbonate precipitation in construction materials: A review, Ecol Eng 36 (2010) 118–136. https://doi.org/10.1016/J.ECOLENG.2009.02.006.

[59] X. Yuan, H. Xu, X. Liu, J. Zhang, J. Li, Q. Liang, B. An, G.M. Paternò, M. Zhang, Y. Tang, C. Zhang, D. Xu, C. Zhong, K. Li, X. Wang, Engineered Living Energy Materials, Interdisciplinary Materials 4 (2025) 412–455. https://doi.org/10.1002/IDM2.12245.

[60] S.J. Park, M. Gazzola, K.S. Park, S. Park, V. Di Santo, E.L. Blevins, J.U. Lind, P.H. Campbell, S. Dauth, A.K. Capulli, F.S. Pasqualini, S. Ahn, A. Cho, H. Yuan, B.M. Maoz, R. Vijaykumar, J.W. Choi, K. Deisseroth, G. V. Lauder, L. Mahadevan, K.K. Parker, Phototactic guidance of a tissue-engineered soft-robotic ray, Science (1979) 353 (2016) 158–162. https://doi.org/10.1126/SCIENCE.AAF4292.

[61] L. Sun, Z. Chen, F. Bian, Y. Zhao, Bioinspired Soft Robotic Caterpillar with Cardiomyocyte Drivers, Adv Funct Mater 30 (2020) 1907820. https://doi.org/10.1002/ADFM.201907820.

[62] L.K. Rivera-Tarazona, Z.T. Campbell, T.H. Ware, Stimuli-responsive engineered living materials, Soft Matter 17 (2021) 785–809. https://doi.org/10.1039/D0SM01905D.

[63] R. Foudazi, R. Zowada, I. Manas-Zloczower, D.L. Feke, Porous Hydrogels: Present Challenges and Future Opportunities, Langmuir 39 (2023) 2092–2111. https://doi.org/10.1021/ACS.LANGMUIR.2C02253.

[64] C.F. Guimarães, R. Ahmed, A.P. Marques, R.L. Reis, U. Demirci, Engineering Hydrogel-Based Biomedical Photonics: Design, Fabrication, and Applications, Advanced Materials 33 (2021) 2006582. https://doi.org/10.1002/ADMA.202006582.

[65] X. Liu, M.E. Inda, Y. Lai, T.K. Lu, X. Zhao, Engineered Living Hydrogels, Advanced Materials 34 (2022) 2201326. https://doi.org/10.1002/ADMA.202201326.

[66] Y. Liu, X. Xia, Z. Liu, M. Dong, The Next Frontier of 3D Bioprinting: Bioactive Materials Functionalized by Bacteria, Small 19 (2023) 2205949. https://doi.org/10.1002/SMLL.202205949.

[67] M.L. Bedell, A.M. Navara, Y. Du, S. Zhang, A.G. Mikos, Polymeric Systems for Bioprinting, Chem Rev 120 (2020) 10744–10792. https://doi.org/10.1021/acs.chemrev.9b00834.

[68] S.S. Kim, H. Utsunomiya, J.A. Koski, B.M. Wu, M.J. Cima, J. Sohn, K. Mukai, L.G. Griffith, J.P. Vacanti, Survival and function of hepatocytes on a novel three-dimensional synthetic biodegradable polymer scaffold with an intrinsic network of channels, Ann Surg 228 (1998) 8–13. https://doi.org/10.1097/00000658-199807000-00002.

[69] V. Mironov, N. Reis, B. Derby, Review: Bioprinting: A Beginning, https://Home.Liebertpub.Com/Ten 12 (2006) 631–634. https://doi.org/10.1089/TEN.2006.12.631.

[70] S. V. Murphy, A. Atala, 3D bioprinting of tissues and organs, Nat Biotechnol 32 (2014) 773–785. https://doi.org/10.1038/NBT.2958.

[71] D. Mallya, M.A. Gadre, S. Varadharajan, K.S. Vasanthan, 3D bioprinting for the construction of drug testing models-development strategies and regulatory concerns, Front Bioeng Biotechnol 13 (2025) 1457872. https://doi.org/10.3389/FBIOE.2025.1457872.

[72] D. Molander, Y. Sbirkov, V. Sarafian, 3D bioprinting as an emerging standard for cancer modeling and drug testing, Folia Medica 64(4): 559–565 64 (2022) 559–565. https://doi.org/10.3897/FOLMED.64.E73419.

[73] X. Pu, Y. Wu, J. Liu, B. Wu, 3D Bioprinting of Microbial-based Living Materials for Advanced Energy and Environmental Applications, Chem & Bio Engineering 1 (2024) 568–592. https://doi.org/10.1021/CBE.4C00024.
[74] L. Sabio, G.J. Day, M. Salmeron-Sanchez, Probiotic-Based Materials as Living Therapeutics, Advanced Materials (2025). https://doi.org/10.1002/ADMA.202508500.
[75] A. Saha, T.G. Johnston, R.T. Shafranek, C.J. Goodman, J.G. Zalatan, D.W. Storti, M.A. Ganter, A. Nelson, Additive Manufacturing of Catalytically Active Living Materials, ACS Appl Mater Interfaces 10 (2018) 13373–13380. https://doi.org/10.1021/acsami.8b02719.
[76] T.G. Johnston, S.F. Yuan, J.M. Wagner, X. Yi, A. Saha, P. Smith, A. Nelson, H.S. Alper, Compartmentalized microbes and co-cultures in hydrogels for on-demand bioproduction and preservation, Nat Commun 11 (2020) 1–11. https://doi.org/10.1038/s41467-020-14371-4.
[77] J. Herzog, L. Franke, Y. Lai, P. Gomez Rossi, J. Sachtleben, D. Weuster-Botz, 3D bioprinting of microorganisms: principles and applications, Bioprocess Biosyst Eng 47 (2024) 443–461. https://doi.org/10.1007/s00449-023-02965-3.
[78] L.M. González, N. Mukhitov, C.A. Voigt, Resilient living materials built by printing bacterial spores, Nature Chemical Biology 2019 16:2 16 (2019) 126–133. https://doi.org/10.1038/s41589-019-0412-5.
[79] S. Zoghi, Advancements in Tissue Engineering: A Review of Bioprinting Techniques, Scaffolds, and Bioinks, Biomed Eng Comput Biol 15 (2024) 11795972241288100. https://doi.org/10.1177/11795972241288099.
[80] B. Yilmaz, A. Al Rashid, Y.A. Mou, Z. Evis, M. Koç, Bioprinting: A review of processes, materials and applications, Bioprinting 23 (2021) e00148. https://doi.org/10.1016/J.BPRINT.2021.E00148.
[81] M. Kandasamy, K. Vijayananth, A. Parasuraman, N. Ayrilmis, 3D Bioprinting of Biomaterials: A Review of Advances in Techniques, Materials, and Applications, Polym Adv Technol 36 (2025) e70324. https://doi.org/10.1002/PAT.70324.
[82] R.L. Reis, M.E. Gomes, A.P. Marques, R. De Filippo, K.C. Young, S.M. Majka, H.T. Ku, J. Rousset, F.J. Richmond, Encyclopedia of Tissue Engineering and Regenerative Medicine: Volumes 1–3, 2019.
[83] Y. Yu, Y. Zhang, J.A. Martin, I.T. Ozbolat, Evaluation of Cell Viability and Functionality in Vessel-like Bioprintable Cell-Laden Tubular Channels, J Biomech Eng 135 (2013). https://doi.org/10.1115/1.4024575.
[84] M. Domingos, F. Intranuovo, T. Russo, R. De Santis, A. Gloria, L. Ambrosio, J. Ciurana, P. Bartolo, The first systematic analysis of 3D rapid prototyped poly(ε-caprolactone) scaffolds manufactured through BioCell printing: the effect of pore size and geometry on compressive mechanical behaviour and *in vitro* hMSC viability, Biofabrication 5 (2013) 045004. https://doi.org/10.1088/1758-5082/5/4/045004.
[85] A.B. Dababneh, I.T. Ozbolat, Bioprinting Technology: A Current State-of-the-Art Review, J Manuf Sci Eng 136 (2014). https://doi.org/10.1115/1.4028512.
[86] Katja Hölzl, 7 Shengmao Lin3, 6, 5 Liesbeth Tytgat4, 5 Sandra Van Vlierberghe4, Linxia Gu3 and, 2 Aleksandr Ovsianikov1, Bioink properties before, during and after 3D bioprinting, Biofabrication 8 (2016) 1–20. https://iopscience.iop.org/article/10.1088/1758-5090/8/3/032002.

[87] M. Müller, E. Öztürk, Ø. Arlov, P. Gatenholm, M. Zenobi-Wong, Alginate Sulfate–Nanocellulose Bioinks for Cartilage Bioprinting Applications, Ann Biomed Eng 45 (2017) 210–223. https://doi.org/10.1007/s10439-016-1704-5.
[88] M. Li, X. Tian, D.J. Schreyer, X. Chen, Effect of needle geometry on flow rate and cell damage in the dispensing-based biofabrication process, Biotechnol Prog 27 (2011) 1777–1784. https://doi.org/10.1002/btpr.679.
[89] W. Liu, M.A. Heinrich, Y. Zhou, A. Akpek, N. Hu, X. Liu, X. Guan, Z. Zhong, X. Jin, A. Khademhosseini, Y.S. Zhang, Extrusion Bioprinting of Shear-Thinning Gelatin Methacryloyl Bioinks, Adv Healthc Mater 6 (2017). https://doi.org/10.1002/adhm.201601451.
[90] D. Patrocinio, V. Galván-Chacón, J.C. Gómez-Blanco, S.P. Miguel, J. Loureiro, M.P. Ribeiro, P. Coutinho, J.B. Pagador, F.M. Sanchez-Margallo, Biopolymers for Tissue Engineering: Crosslinking, Printing Techniques, and Applications, Gels 9 (2023) 890. https://doi.org/10.3390/gels9110890.
[91] X. Cui, D. Dean, Z.M. Ruggeri, T. Boland, Cell damage evaluation of thermal inkjet printed chinese hamster ovary cells, Biotechnol Bioeng 106 (2010) 963–969. https://doi.org/10.1002/BIT.22762.
[92] R. Seetharam, S.K. Sharma, Purification and analysis of recombinant proteins, M. Dekker, New York, 1991.
[93] B. Canfield, S. Diego, C. Holstun, Method and apparatus for reducing the size of drops ejected from a thermal ink jet printhead, (1994).
[94] Method and apparatus for reducing the size of drops ejected from a thermal ink jet printhead, (1994).
[95] S.W. Hock, S. Diego, D.A. Johnson, M.A. Van, Print quality optimization for a color ink-jet printer by using a larger nozzle for the black ink only, (1994).
[96] J.M. Lee, W.L. Ng, W.Y. Yeong, Resolution and shape in bioprinting: Strategizing towards complex tissue and organ printing, Appl Phys Rev 6 (2019). https://doi.org/10.1063/1.5053909/570965.
[97] S. Liu, Y. Chen, Z. Wang, M. Liu, Y. Zhao, Y. Tan, Z. Qu, L. Du, C. Wu, The cutting-edge progress in bioprinting for biomedicine: principles, applications, and future perspectives, MedComm (Beijing) 5 (2024) e753. https://doi.org/10.1002/MCO2.753.
[98] Z. Wang, R. Abdulla, B. Parker, R. Samanipour, S. Ghosh, K. Kim, A simple and high-resolution stereolithography-based 3D bioprinting system using visible light crosslinkable bioinks, Biofabrication 7 (2015) 045009. https://doi.org/10.1088/1758-5090/7/4/045009.
[99] B. Zeng, Z. Cai, J. Lalevée, Q. Yang, H. Lai, P. Xiao, J. Liu, F. Xing, Cytotoxic and cytocompatible comparison among seven photoinitiators-triggered polymers in different tissue cells, Toxicology in Vitro 72 (2021) 105103. https://doi.org/10.1016/J.TIV.2021.105103.
[100] D. Duymaz, İ.C. Karaoğlu, S. Kizilel, Effect of Photoinitiation Process on Photo-Crosslinking of Gelatin Methacryloyl Hydrogel Networks, Macromol Rapid Commun 46 (2025) e00376. https://doi.org/10.1002/MARC.202500376.
[101] A.J. Melchiorri, N. Hibino, C.A. Best, T. Yi, Y.U. Lee, C.A. Kraynak, L.K. Kimerer, A. Krieger, P. Kim, C.K. Breuer, J.P. Fisher, 3D-Printed Biodegradable Polymeric Vascular Grafts, Adv Healthc Mater 5 (2016) 319–325. https://doi.org/10.1002/ADHM.201500725.

[102] W. Ye, H. Li, K. Yu, C. Xie, P. Wang, Y. Zheng, P. Zhang, J. Xiu, Y. Yang, F. Zhang, Y. He, Q. Gao, 3D printing of gelatin methacrylate-based nerve guidance conduits with multiple channels, Mater Des 192 (2020) 108757. https://doi.org/10.1016/J.MATDES.2020.108757.
[103] C. Michas, M.Ç. Karakan, P. Nautiyal, J.G. Seidman, C.E. Seidman, A. Agarwal, K. Ekinci, J. Eyckmans, A.E. White, C.S. Chen, Engineering a living cardiac pump on a chip using high-precision fabrication, Sci Adv 8 (2022) 3791. https://doi.org/10.1126/SCIADV.ABM3791.
[104] A. Marino, O. Tricinci, M. Battaglini, C. Filippeschi, V. Mattoli, E. Sinibaldi, G. Ciofani, A 3D Real-Scale, Biomimetic, and Biohybrid Model of the Blood-Brain Barrier Fabricated through Two-Photon Lithography, Small 14 (2018) 1702959. https://doi.org/10.1002/SMLL.201702959.
[105] C. Dou, V. Perez, J. Qu, A. Tsin, B. Xu, J. Li, A State-of-the-Art Review of Laser-Assisted Bioprinting and its Future Research Trends, ChemBioEng Reviews 8 (2021) 517–534. https://doi.org/10.1002/CBEN.202000037.
[106] V. Keriquel, H. Oliveira, M. Rémy, S. Ziane, S. Delmond, B. Rousseau, S. Rey, S. Catros, J. Amédée, F. Guillemot, J.C. Fricain, In situ printing of mesenchymal stromal cells, by laser-assisted bioprinting, for in vivo bone regeneration applications, Scientific Reports 2017 7:1 7 (2017) 1778-. https://doi.org/10.1038/s41598-017-01914-x.
[107] G. Odian, PRINCIPLES OF POLYMERIZATION Fourth Edition, (n.d.).
[108] M.A. Dubé, E. Saldívar-Guerra, I. Zapata-González, Copolymerization, Handbook of Polymer Synthesis, Characterization, and Processing (2013) 105–125. https://doi.org/10.1002/9781118480793.CH6.
[109] M.M. Alam, K.S. Jack, D.J.T. Hill, A.K. Whittaker, H. Peng, Gradient copolymers — Preparation, properties and practice, Eur Polym J 116 (2019) 394–414. https://doi.org/10.1016/J.EURPOLYMJ.2019.04.028.
[110] J. Park, S. Jang, J.K. Kim, Morphology and microphase separation of star copolymers, J Polym Sci B Polym Phys 53 (2015) 1–21. https://doi.org/10.1002/POLB.23604.
[111] Amphiphilic Block Copolymers, Amphiphilic Block Copolymers (2000). https://doi.org/10.1016/B978-0-444-82441-7.X5000-2.
[112] F. Perin, A. Motta, D. Maniglio, Amphiphilic copolymers in biomedical applications: Synthesis routes and property control, Materials Science and Engineering: C 123 (2021) 111952. https://doi.org/10.1016/J.MSEC.2021.111952.
[113] N.G. Andrade, I.O. Torquato, N.K.B. Lino, O.S. Pillaca-Pullo, N.V.P. Veríssimo, A.M.M. Maia, S.J. Brown, A.M.S. Jorge, V.C. Santos-Ebinuma, T.L. Greaves, I.C. Roberto, J.F.B. Pereira, C.O. Rangel-Yagui, A.M. Lopes, Aqueous biphasic systems based on Pluronics: An overview of the last 10 years, J Mol Liq 428 (2025) 127530. https://doi.org/10.1016/J.MOLLIQ.2025.127530.
[114] D. O'Brien, M. Richardson, S. Kostka, D. Karcher, Examining the Structure-Function Relationship of Block Copolymer Soil Surfactants in Sand-Based Putting Greens, Pesticide Formulation and Delivery Systems: 42nd Volume, Building the Future of Agrochemicals for 2030 and Beyond (2024) 61–80. https://doi.org/10.1520/STP165120230008.
[115] I.R. Schmolka, Artificial skin I. Preparation and properties of pluronic F-127 gels for treatment of burns, J Biomed Mater Res 6 (1972) 571–582. https://doi.org/10.1002/JBM.820060609.

[116] P. Alexandridis, Poly(ethylene oxide)/poly(propylene oxide) block copolymer surfactants, Curr Opin Colloid Interface Sci 2 (1997) 478–489. https://doi.org/10.1016/S1359-0294(97)80095-7.
[117] B. Lindman, Paschalis. Alexandridis, Amphiphilic block copolymers : self-assembly and applications, (2000) 435.
[118] P. Alexandridis, T. Alan Hatton, Poly(ethylene oxide) poly(propylene oxide) poly(ethylene oxide) block copolymer surfactants in aqueous solutions and at interfaces: thermodynamics, structure, dynamics, and modeling, Colloids Surf A Physicochem Eng Asp 96 (1995) 1–46. https://doi.org/10.1016/0927-7757(94)03028-X.
[119] E. Russo, C. Villa, Poloxamer Hydrogels for Biomedical Applications, Pharmaceutics 11 (2019) 671. https://doi.org/10.3390/PHARMACEUTICS11120671.
[120] G. Dumortier, J.L. Grossiord, F. Agnely, J.C. Chaumeil, A review of poloxamer 407 pharmaceutical and pharmacological characteristics, Pharm Res 23 (2006) 2709–2728. https://doi.org/10.1007/S11095-006-9104-4.
[121] Z. Wang, C. Huang, X. Han, S. Li, Z. Wang, J. Huang, H. Liu, Z. Chen, Fabrication of aerogel scaffolds with adjustable macro/micro-pore structure through 3D printing and sacrificial template method for tissue engineering, Mater Des 217 (2022) 110662. https://doi.org/10.1016/J.MATDES.2022.110662.
[122] S.C. Millik, A.M. Dostie, D.G. Karis, P.T. Smith, M. McKenna, N. Chan, C.D. Curtis, E. Nance, A.B. Theberge, A. Nelson, 3D printed coaxial nozzles for the extrusion of hydrogel tubes toward modeling vascular endothelium, Biofabrication 11 (2019) 1–18. https://doi.org/10.1088/1758-5090/ab2b4d.
[123] T.G. Johnston, C.R. Fellin, A. Carignano, A. Nelson, Poly(alkyl glycidyl ether) hydrogels for harnessing the bioactivity of engineered microbes, Faraday Discuss 219 (2019) 58–72. https://doi.org/10.1039/c9fd00019d.
[124] H. Priks, T. Butelmann, Scanning electron microscopy (SEM) protocol for imaging living materials v1, (2020) 1–7. https://doi.org/10.17504/protocols.io.bekcjcsw.
[125] L. Gentile, G. De Luca, F.E. Antunes, C.O. Rossi, G.A. Ranieri, Thermogelation Analysis of F127-Water Mixtures by Physical Chemistry Techniques, (n.d.). https://doi.org/10.3933/ApplRheol-20-52081.
[126] S. V. Murphy, A. Atala, 3D bioprinting of tissues and organs, Nature Biotechnology 2014 32:8 32 (2014) 773–785. https://doi.org/10.1038/nbt.2958.
[127] L. Ouyang, C.B. Highley, C.B. Rodell, W. Sun, J.A. Burdick, 3D Printing of Shear-Thinning Hyaluronic Acid Hydrogels with Secondary Cross-Linking, ACS Biomater Sci Eng 2 (2016) 1743–1751. https://doi.org/10.1021/ACSBIOMATERIALS.6B00158.
[128] F. Della Sala, M. Biondi, D. Guarnieri, A. Borzacchiello, L. Ambrosio, L. Mayol, Mechanical behavior of bioactive poly(ethylene glycol) diacrylate matrices for biomedical application, J Mech Behav Biomed Mater 110 (2020) 103885. https://doi.org/10.1016/J.JMBBM.2020.103885.
[129] M.S.H. Akash, K. Rehman, S. Chen, Pluronic F127-based thermosensitive gels for delivery of therapeutic proteins and peptides, Polymer Reviews 54 (2014) 573–597. https://doi.org/10.1080/15583724.2014.927885.
[130] N.F. Suremann, B.D. McCarthy, W. Gschwind, A. Kumar, B.A. Johnson, L. Hammarström, S. Ott, Molecular Catalysis of Energy Relevance in Metal–Organic Frameworks: From Higher Coordination Sphere to System Effects, Chem Rev 123 (2023) 6545–6611. https://doi.org/10.1021/ACS.CHEMREV.2C00587.

[131] B. Schmieg, M. Nguyen, M. Franzreb, Simulative Minimization of Mass Transfer Limitations Within Hydrogel-Based 3D-Printed Enzyme Carriers, Front Bioeng Biotechnol 8 (2020) 365. https://doi.org/10.3389/FBIOE.2020.00365/FULL.
[132] A.N. Gent, On the Relation between Indentation Hardness and Young's Modulus, Rubber Chemistry and Technology 31 (1958) 896–906. https://doi.org/10.5254/1.3542351.
[133] H.J. Qi, K. Joyce, M.C. Boyce, Durometer Hardness and the Stress-Strain Behavior of Elastomeric Materials, Rubber Chemistry and Technology 76 (2003) 419–435. https://doi.org/10.5254/1.3547752.
[134] I.M. Meththananda, S. Parker, M.P. Patel, M. Braden, The relationship between Shore hardness of elastomeric dental materials and Young's modulus, Dental Materials 25 (2009) 956–959. https://doi.org/10.1016/J.DENTAL.2009.02.001.
[135] H. Sugiyama, K. ichi Katoh, N. Sekine, Y. Sekine, T. Watanabe, T. Ikeda-Fukazawa, Effects of hydrophilic groups of polymer on change in hydrogen-bonding structure of water in hydrogels during dehydration, Chem Phys Lett 856 (2024) 141655. https://doi.org/10.1016/J.CPLETT.2024.141655.
[136] E.O. Nachaki, F.M. Leonik, D.G. Kuroda, Effect of the N-Alkyl Side Chain on the Amide-Water Interactions, Journal of Physical Chemistry B 126 (2022) 8290–8299. https://doi.org/10.1021/acs.jpcb.2c04988.
[137] M.N. Leiske, B.G. De Geest, R. Hoogenboom, Impact of the polymer backbone chemistry on interactions of amino-acid-derived zwitterionic polymers with cells, Bioact Mater 24 (2023) 524–534. https://doi.org/10.1016/J.BIOACTMAT.2023.01.005.
[138] S. Hezaveh, S. Samanta, A. De Nicola, G. Milano, D. Roccatano, Understanding the interaction of block copolymers with DMPC lipid bilayer using coarse-grained molecular dynamics simulations, Journal of Physical Chemistry B 116 (2012) 14333–14345. https://doi.org/10.1021/jp306565e.
[139] J.J. Turner, J.C. Ewald, J.M. Skotheim, Cell size control in yeast, Current Biology 22 (2012). https://doi.org/10.1016/j.cub.2012.02.041.
[140] K.M. Schmoller, J.M. Skotheim, The Biosynthetic Basis of Cell Size Control, Trends Cell Biol 25 (2015) 793–802. https://doi.org/10.1016/j.tcb.2015.10.006.
[141] H. Yamashita, N. Kakuta, D. Kawashima, Y. Yamada, Measurement of temperature-dependent diffusion coefficients of aqueous solutions by near-infrared simultaneous imaging of temperature and concentration, Biomed Phys Eng Express 4 (2018). https://doi.org/10.1088/2057-1976/aab645.
[142] S.C. Li, P.M. Kane, The yeast lysosome-like vacuole: Endpoint and crossroads, Biochim Biophys Acta Mol Cell Res 1793 (2009) 650–663. https://doi.org/10.1016/j.bbamcr.2008.08.003.
[143] A. Illarionov, P.J. Lahtvee, R. Kumar, Potassium and Sodium Salt Stress Characterization in the Yeasts Saccharomyces cerevisiae, Kluyveromyces marxianus, and Rhodotorula toruloides, Appl Environ Microbiol 87 (2021) 1–16. https://doi.org/10.1128/AEM.03100-20.

APPENDIX

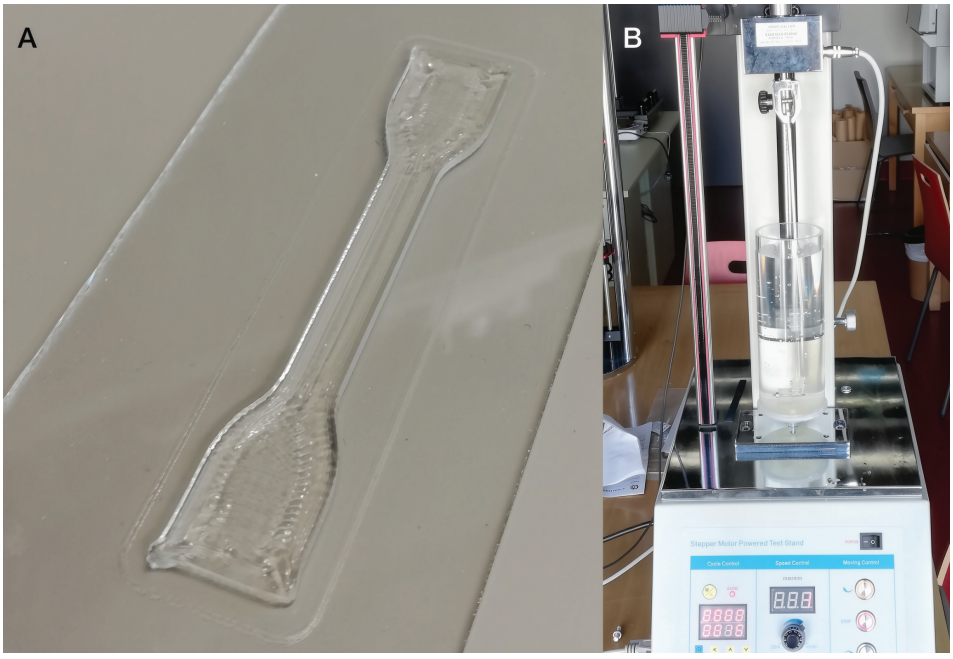

Figure A1. 3D printed dogbone ASTM D412 A (50% reduced scale) (A); universal testing machine with PBS water bath (B) [VI].

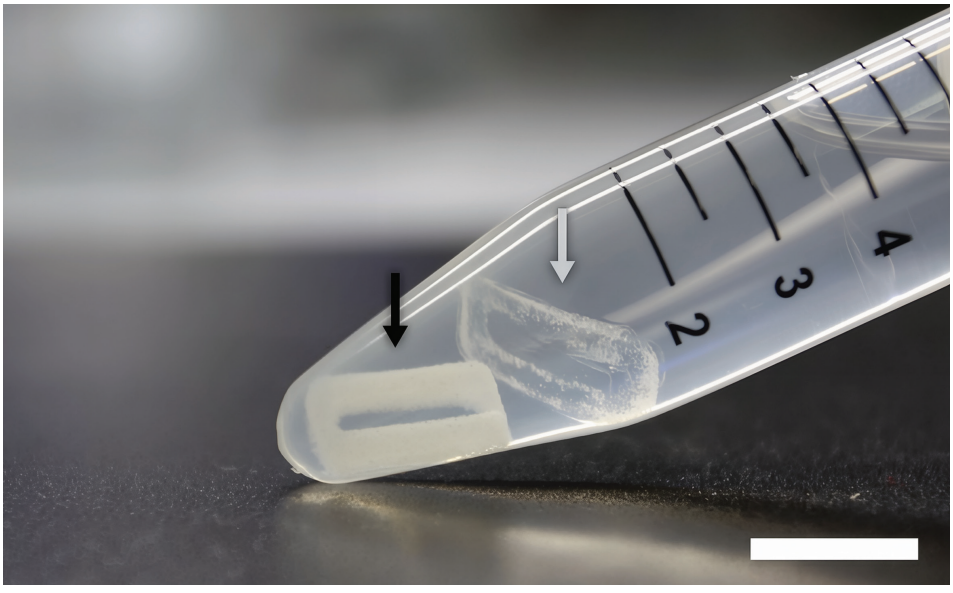

Figure A2. Separation of the outer layer. Photo of F127-DMA hydrogel after 14 day of incubation. Full separation of inner (black arrow) and outer (grey arrow) layer. Scale bar: 10 mm [I].

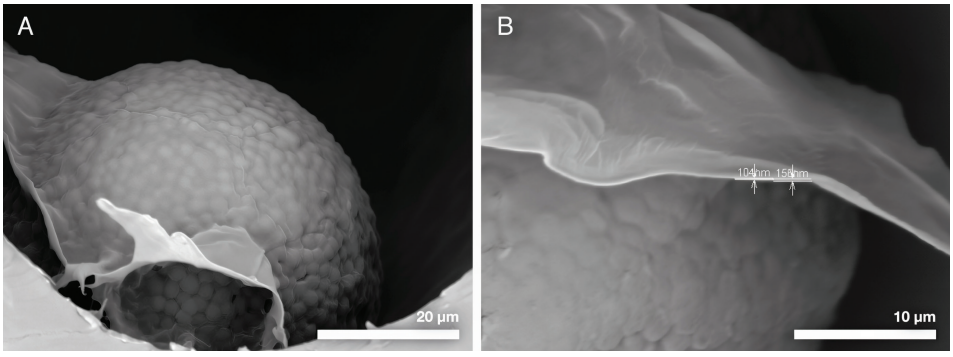

Figure A3. SEM micrographs of organic coating around yeast colony (A) and the thickness of thin film (B) in F127-based hydrogels [I].

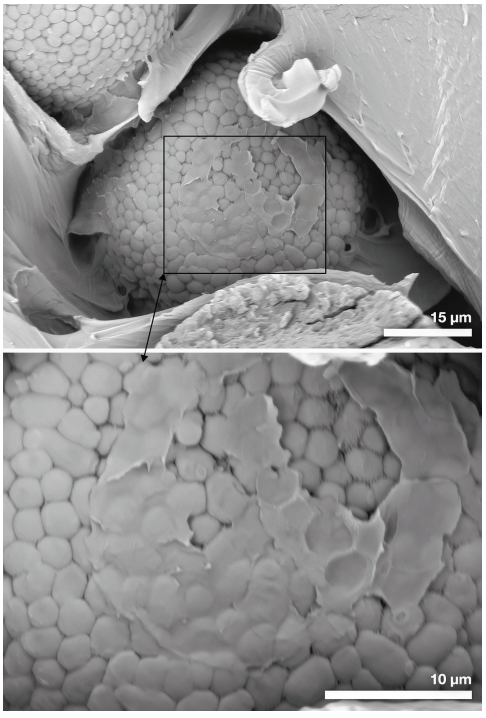

Figure A4. Polymer coating remnants on colony surfaces. Remnants began to appear after the colony reached a certain size (60–80 µm) in F127-based materials [I].

SUMMARY IN ESTONIAN

Elu mitsellaarsetel hüdrogeelidel põhinevates 3D trükitud elusmaterjalides

Aastakümneid on üleilmne majandus järginud lineaarset majandusmudelit – võta, kasuta, viska ära. See lähenemine on olnud lühiajaliselt väga tõhus, kuid on pikaajaliselt keskkonnale laastav. Fossiilkütused on käivitanud meie tööstuse, plastid on kujundanud meie maailma ning tarbimiskultuur on loonud hiiglaslikud jäätmemäed. See areng on aga tulnud kalli hinnaga: tõusvad temperatuurid, ebastabiilsed ilmamustrid ja degradeerunud ökosüsteemid. Paljude jaoks peitub jätkusuutlik lahendus ringbiomajanduse kontseptsioonis, kus bioloogilised ressursid asendavad fossiilkütused tööstuse selgroona ning ressursse hoitakse ringluses võimalikult kaua.

Niisuguse ülemineku keskmes on biotehnoloogia. Elusad mikroorganismid (näiteks bakterid, pärmid, vetikad) ja eukarüootsed rakud (näiteks imetajarakud) – võivad toimida miniatuursete tehastena, mis muudavad taastuvad lähteained väärtuslikeks toodeteks. Geenitehnoloogia ja sünteetilise bioloogia areng on võimaldanud neid elusaid süsteeme üha suurema täpsusega suunata tööstus- ja keskkonnaeesmärkide saavutamiseks, laiendades bioloogilisel teel saavutatavate toodete ja funktsioonide spektrit.

Kuid ka elusrakkudel on piirangud. Tootlikkuse säilitamiseks vajavad nad tavaliselt hoolikalt kontrollitud ja steriilset keskkonda. Aja jooksul, eriti keerukates või muutuvates tingimustes, võib nende jõudlus geneetilise ebastabiilsuse ja mutatsioonide kuhjumise tõttu halveneda, viies funktsionaalsuse kaoni või kontrollimatu paljunemiseni. Lisaks on bioturvalisuse tagamine ja geneetilise materjali lekkimise vältimine looduslikesse ökosüsteemidesse jätkuv väljakutse. Need piirangud rõhutavad materjalipõhiste strateegiate vajadust – näiteks rakkude kapseldamine konstrueeritud elusmaterjalidesse (ingl. k. *engineered living materials*, ELMs), mis pakuvad füüsilist kaitset, vabanemisekontrolli, keskkonnatingimuste puhverdamist ja stabiilseid mikrokeskkondi, suurendamaks nende sünteetiliste bioloogiliste süsteemide töökindlust. Elusmaterjalides rakendamiseks on uuritud mitmesuguseid biopõhiseid ja biopolümeerseid materjale. Paraku ei ole enamik neist bioloogiliselt inertsed ning võivad seetõttu olla vastuvõtlikud mikroobsele degradeerumisele või nende samade organismide põhjustatud ensümaatilisele lagunemisele, keda nad on mõeldud majutama, mis omakorda piirab nende kasutamist pikaajalistes biotootmise protsessides.

Käesolevas töös uuriti UV-ristsidestatavaid mitsellaarseid hüdrogeele – eeskätt F127-BUM, F127-DMA ja PGE-DMA – kui struktuurseid platvorme ELMide 3D printimiseks. Töö keskendus sellele, kuidas mitsellaarsed hüdrogeelid suunavad rakkude ruumilist organiseeritust, paljunemist, fenotüüpi ja metabolismi. Laiem eesmärk oli määratleda disainireeglid skaleeritavate, ruumiliselt organiseeritud ja metaboolselt programmeeritavate elussüsteemide loomiseks.

Esmalt uuriti nende materjalide trükitavust ja trükitud objektide struktuurset täpsust. Kooskõlas varasemate kirjeldustega, sai kõiki uuritud hüdrogeele ekstrudeerida, UV-ristsiduda ning vormida keeruka geomeetriaga 3D konstruktsioonideks. Konstruktsiooni erinevatesse sektsioonidesse trükitud mikroobsete populatsioonide (bakterid, pärmid, vetikad) vahel säilisid selged piirpinnad, mis näitas, et mitsellaarsed hüdrogeelid suudavad toetada ruumiliselt eristatud ja mitmeliigilisi mikroobikooslusi. Uuritud materjalidel esineb lahustes märkimisväärne järelpundumine ning nad on temperatuuri suhtes tundlikud, mille tagajärjel muutub nende veesisaldus ja kõvadus. Seega ei määra trükitud konstruktsiooni lõplikku geomeetriat ja mehaanilisi omadusi üksnes printimise etapp, vaid ka sellele järgnev tasakaalustumine töökeskonnas, mida tuleb konstruktsiooni disainis arvesse võtta.

Rakuvabad katsed näitasid, et ristsidestatud hüdrogeelid püsisid kultiveerimiskeskkonnas struktuurselt stabiilsed – ilma mõõdetava roome, massikao või nähtava degradatsioonita. See lõi võrdlusbaasi, mille suhtes sai bioloogilisi efekte – rakkudest tingitud deformatsioon, pundumine, massi suurenemine – seostada rakudega, mitte materjali enda omaduste muutumisega.

Seejärel hinnati süsteemide bioloogilist talitlust. F127-BUM hüdrogeelmaatriks toetas kõrget elujõulisust (>90%) nii pärmi, bakterite kui vetikate puhul. Rakud jäid struktuuri piires oma trükitud piirkondadesse, kuid aeg-ajalt lekkis struktuuri väliskihist rakke ümbritsevasse keskkonda. See viitab, et hüdrogeelivõrk toimib selektiivse barjäärina: see lubab toitainete transporti, kuid piirab rakkude migratsiooni struktuuri sees. Selline omadus võimaldab mikroorganismide kolokaliseerimist lähestikku ilma kontrollimatu levikuta.

Kasvuanalüüs näitas, et kapseldatud pärm ei paljune mitsellaarses struktuuris ühtlaselt. Kolooniad struktuuri perifeerias kasvasid kiiremini ja saavutasid suurema läbimõõdu kui sügavamal materjali sees paiknevad kolooniad, kus toiteainete difusioon-kontrollitud kättesaadavus oli piiratud. Erinevates hüdrogeelides eristusid ruumilised kasvumustrid: F127-põhised süsteemid soodustasid sfäärilise koloonia moodustumist, samas kui PGE-DMA toetas ebakorrapärasemat käävjat kasvu. Need tulemused näitavad, et hüdrogeeli koostis ja struktuur kujundavad lokaalseid „ökoloogiaid“ materjali sees. Samuti selgus, et pelgalt paksemate struktuuride printimine ei vii proportsionaalselt suurema tootliku biomassi tekkimiseni, sest piiravaks teguriks on massiülekanne.

Rakkude peetumine maatriksis ja konstruktsiooni vastupidavus sõltuvad mehaanilistest omadustest. Peetusaeg erines materjalide lõikes ja korreleerus pigem sitkuse ja purunemiskindlusega kui lihtsalt jäikusega. Mehaanilised katsed ja modelleerimine näitasid, et paisuvad kolooniad tekitavad pingekontsentratsioonid, mis ületavad maatriksi lokaalse purunemisläve. Rakkude lekkimine on seega eeskätt mehaaniline, mitte bioloogiline rike: rakud pääsevad välja siis, kui lokaalsed pinged põhjustavad hüdrogeelmaatriksis pragusid, mikropragusid või rebendeid. ELM-ide tööea pikendamiseks on vaja tõsta materjali purunemiskindlust ja võimet pingeid hajutada, mitte lihtsalt jäikust suurendada.

Difusioonikatsed näitasid, et glükoosi ja etanooli difusioon on F127-põhises hüdrogeelis oluliselt aeglasem kui vees, ning metaboolsed uuringud tõid esile, et

hapniku transport kapseldatud piirkondadesse on tugevalt piiratud. Selle tulemusena võttis ja säilitas pärm F127-BUM-is valdavalt fermentatiivse ainevahetusseisundi isegi tingimustes, kus sama tüve suspensioonikultuurid olid respiratoorsed. Nii piirab hüdrogeeli maatriks ise ainevahetusseisundit füüsilise takistuse ja hapniku piiramise kaudu, ilma igasuguse geneetilise sekkumise või välise õhustamise kontrollita.

Lõpuks demonstreeriti neid põhimõtteid rakenduslikus kontekstis. Õllepärmi rakkudega laetud 3D-trükitud konstruktsioonid andsid identsetes tingimustes kõrgema etanoolisaagise ja selgema lõpp-toote kui ekvivalentne suspensioonikultuur. See kinnitab, et mitsellaarsetel hüdrogeelidel põhinevad ELM-id toimivad metaboolselt häälestatud biokatalüütiliste üksustena.

Kokkuvõttes näitab käesolev doktoritöö, et mitsellaarsed hüdrogeelid ei ole ELMides pelgalt passiivsed toed, vaid aktiivsed regulaatorid, mis juhivad ruumilist mustristumist, struktuurilist eraldamist, rakkude püsivust ja ainevahetust. Tulemused sõnastavad praktilised disainieeskirjad, mis seovad trükitavuse, mehaanilise käitumise ja ainetranspordi bioloogilise funktsiooniga, luues aluse töökindlamate, ruumiliselt struktureeritud ja programmeeritavate ELM-ide arendamiseks tulevasteks bioprotsessideks.

ACKNOWLEDGEMENTS

I would like to thank all co-authors of the publications on which this thesis is based for their contributions, constructive discussions, and collaboration throughout this work. I am also deeply grateful to my family and friends for their encouragement and patience during this journey. In particular, I thank my son, Johannes, who has brought so much joy, warmth, and optimism — reminding me to keep perspective and move forward with a smile.

I am thankful to everyone I have been honoured to learn from and work with during my studies at the Institute of Technology. I also appreciate the support of my colleagues and the students I had the privilege to supervise.

Finally, I extend my deepest gratitude to my supervisor, Prof. Tarmo Tamm, for his unwavering support throughout these years. His trust and encouragement gave me the freedom to explore ideas, take risks, and develop my own approach to research and writing. At the same time, his guidance and steady oversight ensured I stayed focused and moved forward with purpose.

PUBLICATIONS

CURRICULUM VITAE

Name:	Hans Priks
Date of birth:	October 2, 1987
Citizenship:	Estonian
Contact:	hans.priks@ut.ee

Education

2017–...	Doctoral studies in Engineering and Technology, University of Tartu
2013–2016	M.Sc. Materials Science, University of Tartu
2007–2013	B.Sc. Applied Chemistry and Biotechnology, Tallinn University of Technology

Professional employment

01.07.2023–	University of Tartu, Faculty of Science and Technology, Institute of Technology, Junior Research Fellow in Materials Science
01.09.2022–30.06.2023	University of Tartu, Faculty of Science and Technology, Institute of Technology, Project Manager
15.10.2019–30.06.2021	University of Tartu, Faculty of Science and Technology, Institute of Technology, Specialist of Additive Manufacturing
01.02.2019–31.12.2019	BiotaTec LLC, Junior Research Fellow
01.11.2014–2017	MolCode LTD, Junior Research Fellow

Scientific publications

Priks, H., Zadin, V., Talgre, I. R., Zekker, I., & Tamm, T. (2025). Linking physical properties of micellar hydrogels to engineered living material performance. Materials & Design, 256, 114347. https://doi.org/10.1016/J.MATDES.2025.114347

Priks, H., Zekker, I., Nava, A. I. M., Kumar, R., Das, S., Jaagura, M., Mamun, F. al, Bhowmick, G. D., Tamm, T., & Tenno, T. (2024). Enhanced anammox-mediated nitrogen removal in bioelectrochemical systems at prolonged negative electrode potentials. Environmental Science and Pollution Research 2024 31:54, 31(54), 63312–63324. https://doi.org/10.1007/S11356-024-35405-0

Rebane, I., **Priks, H.**, Levin, K. J., Sarigül, İ., Mäeorg, U., Johanson, U., Piirimägi, P., Tenson, T., & Tamm, T. (2023). Microbial growth and adhesion of Escherichia coli in elastomeric silicone foams with commonly used additives. *Scientific Reports 2023 13:1*, *13*(1), 8541-. https://doi.org/10.1038/s41598-023-35239-9

Evard, H., **Priks, H.**, Saar, I., Aavola, H., Tamm, T., & Leito, I. (2021). A new direction in microfluidics: Printed porous materials. *Micromachines*, *12*(6), 671. https://doi.org/10.3390/MI12060671/S1

Butelmann, T., **Priks, H.**, Parent, Z., Johnston, T. G., Tamm, T., Nelson, A., Lahtvee, P. J., & Kumar, R. (2021). Metabolism Control in 3D-Printed Living Materials Improves Fermentation. *ACS Applied Bio Materials*, *4*(9), 7195–7203. https://doi.org/10.1021/ACSABM.1C00754

Zekker, I., Raudkivi, M., Artemchuk, O., Rikmann, E., **Priks, H.**, Jaagura, M., & Tenno, T. (2021). Mainstream-sidestream wastewater switching promotes anammox nitrogen removal rate in organic-rich, low-temperature streams. *Environmental Technology (United Kingdom)*, *42*(19), 3073–3082. https://doi.org/10.1080/09593330.2020.1721566

Johnston, T. G., Fillman, J. P., **Priks, H.**, Butelmann, T., Tamm, T., Kumar, R., Lahtvee, P. J., & Nelson, A. (2020). Cell-Laden Hydrogels for Multikingdom 3D Printing. *Macromolecular Bioscience*, *20*(8), 2000121. https://doi.org/10.1002/MABI.202000121

Elhi, F., **Priks, H.**, Rinne, P., Kaldalu, N., Žusinaite, E., Johanson, U., Aabloo, A., Tamm, T., & Põhako-Esko, K. (2020). Electromechanically active polymer actuators based on biofriendly choline ionic liquids. *Smart Materials and Structures*, *29*(5), 055021. https://doi.org/10.1088/1361-665X/AB7F24

Priks, H., Butelmann, T., Illarionov, A., Johnston, T. G., Fellin, C., Tamm, T., Nelson, A., Kumar, R., & Lahtvee, P. J. (2020). Physical Confinement Impacts Cellular Phenotypes within Living Materials. *ACS Applied Bio Materials*, *3*(7), 4273–4281. https://doi.org/10.1021/ACSABM.0C00335

Zekker, I., Bhowmick, G. D., **Priks, H.**, Nath, D., Rikmann, E., Jaagura, M., Tenno, T., Tämm, K., & Ghangrekar, M. M. (2020). ANAMMOX-denitrification biomass in microbial fuel cell to enhance the electricity generation and nitrogen removal efficiency. *Biodegradation 2020 31:4*, *31*(4), 249–264. https://doi.org/10.1007/S10532-020-09907-W

ELULOOKIRJELDUS

Nimi:	Hans Priks
Sünniaeg:	2.10.1987
Kodakondsus:	Eesti
Kontakt:	hans.priks@ut.ee

Hariduskäik

2017–...	Doktoriõpe, Tehnika ja tehnoloogia, Tartu Ülikool
2013–2016	M.Sc. Materjaliteadus, Tartu Ülikool
2007–2013	B.Sc. Rakenduskeemia ja Biotehnoloogia, Tallinna Tehnikaülikool

Erialane teenistuskäik

01.07.2023–	Tartu Ülikool, Loodus- ja täppisteaduste valdkond, tehnoloogiainstituut, materjaliteaduse nooremteadur
01.09.2022–30.06.2023	Tartu Ülikool, Loodus- ja täppisteaduste valdkond, tehnoloogiainstituut, projektijuht
15.10.2019–30.06.2021	Tartu Ülikool, Loodus- ja täppisteaduste valdkond, tehnoloogiainstituut, kihtlisandustehnoloogia spetsialist
01.02.2019–31.12.2019	BiotaTec OÜ, Nooremteadur
01.11.2014–2017	MolCode AS, Nooremteadur

Teaduspublikatsioonid

Priks, H., Zadin, V., Talgre, I. R., Zekker, I., & Tamm, T. (2025). Linking physical properties of micellar hydrogels to engineered living material performance. Materials & Design, 256, 114347. https://doi.org/10.1016/J.MATDES.2025.114347

Priks, H., Zekker, I., Nava, A. I. M., Kumar, R., Das, S., Jaagura, M., Mamun, F. al, Bhowmick, G. D., Tamm, T., & Tenno, T. (2024). Enhanced anammox-mediated nitrogen removal in bioelectrochemical systems at prolonged negative electrode potentials. Environmental Science and Pollution Research 2024 31:54, 31(54), 63312–63324. https://doi.org/10.1007/S11356-024-35405-0

Rebane, I., **Priks, H.**, Levin, K. J., Sarigül, İ., Mäeorg, U., Johanson, U., Piirimägi, P., Tenson, T., & Tamm, T. (2023). Microbial growth and adhesion of Escherichia coli in elastomeric silicone foams with commonly used additives. *Scientific Reports 2023 13:1*, *13*(1), 8541-. https://doi.org/10.1038/s41598-023-35239-9

Evard, H., **Priks, H.**, Saar, I., Aavola, H., Tamm, T., & Leito, I. (2021). A new direction in microfluidics: Printed porous materials. *Micromachines*, *12*(6), 671. https://doi.org/10.3390/MI12060671/S1

Butelmann, T., **Priks, H.**, Parent, Z., Johnston, T. G., Tamm, T., Nelson, A., Lahtvee, P. J., & Kumar, R. (2021). Metabolism Control in 3D-Printed Living Materials Improves Fermentation. *ACS Applied Bio Materials*, *4*(9), 7195–7203. https://doi.org/10.1021/ACSABM.1C00754

Zekker, I., Raudkivi, M., Artemchuk, O., Rikmann, E., **Priks, H.**, Jaagura, M., & Tenno, T. (2021). Mainstream-sidestream wastewater switching promotes anammox nitrogen removal rate in organic-rich, low-temperature streams. *Environmental Technology (United Kingdom)*, *42*(19), 3073–3082. https://doi.org/10.1080/09593330.2020.1721566

Johnston, T. G., Fillman, J. P., **Priks, H.**, Butelmann, T., Tamm, T., Kumar, R., Lahtvee, P. J., & Nelson, A. (2020). Cell-Laden Hydrogels for Multikingdom 3D Printing. *Macromolecular Bioscience*, *20*(8), 2000121. https://doi.org/10.1002/MABI.202000121

Elhi, F., **Priks, H.**, Rinne, P., Kaldalu, N., Žusinaite, E., Johanson, U., Aabloo, A., Tamm, T., & Põhako-Esko, K. (2020). Electromechanically active polymer actuators based on biofriendly choline ionic liquids. *Smart Materials and Structures*, *29*(5), 055021. https://doi.org/10.1088/1361-665X/AB7F24

Priks, H., Butelmann, T., Illarionov, A., Johnston, T. G., Fellin, C., Tamm, T., Nelson, A., Kumar, R., & Lahtvee, P. J. (2020). Physical Confinement Impacts Cellular Phenotypes within Living Materials. *ACS Applied Bio Materials*, *3*(7), 4273–4281. https://doi.org/10.1021/ACSABM.0C00335

Zekker, I., Bhowmick, G. D., **Priks, H.**, Nath, D., Rikmann, E., Jaagura, M., Tenno, T., Tämm, K., & Ghangrekar, M. M. (2020). ANAMMOX-denitrification biomass in microbial fuel cell to enhance the electricity generation and nitrogen removal efficiency. *Biodegradation 2020 31:4*, *31*(4), 249–264. https://doi.org/10.1007/S10532-020-09907-W

DISSERTATIONES TECHNOLOGIAE UNIVERSITATIS TARTUENSIS

1. **Imre Mäger**. Characterization of cell-penetrating peptides: Assessment of cellular internalization kinetics, mechanisms and bioactivity. Tartu 2011, 132 p.
2. **Taavi Lehto**. Delivery of nucleic acids by cell-penetrating peptides: application in modulation of gene expression. Tartu 2011, 155 p.
3. **Hannes Luidalepp**. Studies on the antibiotic susceptibility of *Escherichia coli*. Tartu 2012, 111 p.
4. **Vahur Zadin**. Modelling the 3D-microbattery. Tartu 2012, 149 p.
5. **Janno Torop**. Carbide-derived carbon-based electromechanical actuators. Tartu 2012, 113 p.
6. **Julia Suhorutšenko**. Cell-penetrating peptides: cytotoxicity, immunogenicity and application for tumor targeting. Tartu 2012, 139 p.
7. **Viktoryia Shyp**. G nucleotide regulation of translational GTPases and the stringent response factor RelA. Tartu 2012, 105 p.
8. **Mardo Kõivomägi**. Studies on the substrate specificity and multisite phosphorylation mechanisms of cyclin-dependent kinase Cdk1 in *Saccharomyces cerevisiae*. Tartu, 2013, 157 p.
9. **Liis Karo-Astover**. Studies on the Semliki Forest virus replicase protein nsP1. Tartu, 2013, 113 p.
10. **Piret Arukuusk**. NickFects–novel cell-penetrating peptides. Design and uptake mechanism. Tartu, 2013, 124 p.
11. **Piret Villo**. Synthesis of acetogenin analogues. Asymmetric transfer hydrogenation coupled with dynamic kinetic resolution of α-amido-β-keto esters. Tartu, 2013, 151 p.
12. **Villu Kasari**. Bacterial toxin-antitoxin systems: transcriptional cross-activation and characterization of a novel *mqsRA* system. Tartu, 2013, 108 p.
13. **Margus Varjak**. Functional analysis of viral and host components of alphavirus replicase complexes. Tartu, 2013, 151 p.
14. **Liane Viru**. Development and analysis of novel alphavirus-based multifunctional gene therapy and expression systems. Tartu, 2013, 113 p.
15. **Kent Langel**. Cell-penetrating peptide mechanism studies: from peptides to cargo delivery. Tartu, 2014, 115 p.
16. **Rauno Temmer**. Electrochemistry and novel applications of chemically synthesized conductive polymer electrodes. Tartu, 2014, 206 p.
17. **Indrek Must**. Ionic and capacitive electroactive laminates with carbonaceous electrodes as sensors and energy harvesters. Tartu, 2014, 133 p.
18. **Veiko Voolaid**. Aquatic environment: primary reservoir, link, or sink of antibiotic resistance? Tartu, 2014, 79 p.
19. **Kristiina Laanemets**. The role of SLAC1 anion channel and its upstream regulators in stomatal opening and closure of *Arabidopsis thaliana.* Tartu, 2015, 115 p.

20. **Kalle Pärn**. Studies on inducible alphavirus-based antitumour strategy mediated by site-specific delivery with activatable cell-penetrating peptides. Tartu, 2015, 139 p.
21. **Anastasia Selyutina**. When biologist meets chemist: a search for HIV-1 inhibitors. Tartu, 2015, 172 p.
22. **Sirle Saul**. Towards understanding the neurovirulence of Semliki Forest virus. Tartu, 2015, 136 p.
23. **Marit Orav**. Study of the initial amplification of the human papillomavirus genome. Tartu, 2015, 132 p.
24. **Tormi Reinson**. Studies on the Genome Replication of Human Papillomaviruses. Tartu, 2016, 110 p.
25. **Mart Ustav Jr**. Molecular Studies of HPV-18 Genome Segregation and Stable Replication. Tartu, 2016, 152 p.
26. **Margit Mutso**. Different Approaches to Counteracting Hepatitis C Virus and Chikungunya Virus Infections. Tartu, 2016, 184 p.
27. **Jelizaveta Geimanen**. Study of the Papillomavirus Genome Replication and Segregation. Tartu, 2016, 168 p.
28. **Mart Toots**. Novel Means to Target Human Papillomavirus Infection. Tartu, 2016, 173 p.
29. **Kadi-Liis Veiman**. Development of cell-penetrating peptides for gene delivery: from transfection in cell cultures to induction of gene expression *in vivo*. Tartu, 2016, 136 p.
30. **Ly Pärnaste**. How, why, what and where: Mechanisms behind CPP/cargo nanocomplexes. Tartu, 2016, 147 p.
31. **Age Utt**. Role of alphavirus replicase in viral RNA synthesis, virus-induced cytotoxicity and recognition of viral infections in host cells. Tartu, 2016, 183 p.
32. **Veiko Vunder**. Modeling and characterization of back-relaxation of ionic electroactive polymer actuators. Tartu, 2016, 154 p.
33. **Piia Kivipõld**. Studies on the Role of Papillomavirus E2 Proteins in Virus DNA Replication. Tartu, 2016, 118 p.
34. **Liina Jakobson**. The roles of abscisic acid, CO_2, and the cuticle in the regulation of plant transpiration. Tartu, 2017, 162 p.
35. **Helen Isok-Paas**. Viral-host interactions in the life cycle of human papillomaviruses. Tartu, 2017, 158 p.
36. **Hanna Hõrak**. Identification of key regulators of stomatal CO_2 signalling via O_3-sensitivity. Tartu, 2017, 260 p.
37. **Jekaterina Jevtuševskaja**. Application of isothermal amplification methods for detection of *Chlamydia trachomatis* directly from biological samples. Tartu, 2017, 96 p.
38. **Ülar Allas**. Ribosome-targeting antibiotics and mechanisms of antibiotic resistance. Tartu, 2017, 152 p.
39. **Anton Paier**. Ribosome Degradation in Living Bacteria. Tartu, 2017, 108 p.
40. **Vallo Varik**. Stringent Response in Bacterial Growth and Survival. Tartu, 2017, 101 p.

41. **Pavel Kudrin**. In search for the inhibitors of *Escherichia coli* stringent response factor RelA. Tartu, 2017, 138 p.
42. **Liisi Henno**. Study of the human papillomavirus genome replication and oligomer generation. Tartu, 2017, 144 p.
43. **Katrin Krõlov**. Nucleic acid amplification from crude clinical samples exemplified by *Chlamydia trachomatis* detection in urine. Tartu, 2018, 118 p.
44. **Eve Sankovski**. Studies on papillomavirus transcription and regulatory protein E2. Tartu, 2018, 113 p.
45. **Morteza Daneshmand**. Realistic 3D Virtual Fitting Room. Tartu, 2018, 233 p.
46. **Fatemeh Noroozi**. Multimodal Emotion Recognition Based Human-Robot Interaction Enhancement. Tartu, 2018, 113 p.
47. **Krista Freimann**. Design of peptide-based vector for nucleic acid delivery in vivo. Tartu, 2018, 103 p.
48. **Rainis Venta**. Studies on signal processing by multisite phosphorylation pathways of the *S. cerevisiae* cyclin-dependent kinase inhibitor Sic1. Tartu, 2018, 155 p.
49. **Inga Põldsalu**. Soft actuators with ink-jet printed electrodes. Tartu, 2018, 85 p.
50. **Kadri Künnapuu**. Modification of the cell-penetrating peptide PepFect14 for targeted tumor gene delivery and reduced toxicity. Tartu, 2018, 114 p.
51. **Toomas Mets**. RNA fragmentation by MazF and MqsR toxins of *Escherichia coli.* Tartu, 2019, 119 p.
52. **Kadri Tõldsepp**. The role of mitogen-activated protein kinases MPK4 and MPK12 in CO_2-induced stomatal movements. Tartu, 2019, 259 p.
53. **Pirko Jalakas**. Unravelling signalling pathways contributing to stomatal conductance and responsiveness. Tartu, 2019, 120 p.
54. **S. Sunjai Nakshatharan**. Electromechanical modelling and control of ionic electroactive polymer actuators. Tartu, 2019, 165 p.
55. **Eva-Maria Tombak**. Molecular studies of the initial amplification of the oncogenic human papillomavirus and closely related nonhuman primate papillomavirus genomes. Tartu, 2019, 150 p.
56. **Meeri Visnapuu**. Design and physico-chemical characterization of metal-containing nanoparticles for antimicrobial coatings. Tartu, 2019, 138 p.
57. **Jelena Beljantseva**. Small fine-tuners of the bacterial stringent response – a glimpse into the working principles of Small Alarmone Synthetases. Tartu, 2020, 104 p.
58. **Egon Urgard**. Potential therapeutic approaches for modulation of inflammatory response pathways. Tartu, 2020, 120 p.
59. **Sofia Raquel Alves Oliveira**. HPLC analysis of bacterial alarmone nucleotide (p)ppGpp and its toxic analogue ppApp. Tartu, 2020, 122 p.
60. **Mihkel Örd**. Ordering the phosphorylation of cyclin-dependent kinase Cdk1 substrates in the cell cycle. Tartu, 2021, 228 p.
61. **Fred Elhi**. Biocompatible ionic electromechanically active polymer actuator based on biopolymers and non-toxic ionic liquids. Tartu, 2021, 140 p.

62. **Liisi Talas**. Reconstructing paleo-diversity, dynamics and response of eukaryotes to environmental change over the Late-Glacial and Holocene period in lake Lielais Svētiņu using sedaDNA. Tartu, 2021, 118 p.
63. **Livia Matt**. Novel isosorbide-based polymers. Tartu, 2021, 118 p.
64. **Koit Aasumets**. The dynamics of human mitochondrial nucleoids within the mitochondrial network. Tartu, 2021, 104 p.
65. **Faiza Summer**. Development and optimization of flow electrode capacitor technology. Tartu, 2022, 109 p.
66. **Olavi Reinsalu**. Cancer-testis antigen MAGE-A4 is incorporated into extracellular vesiclesand is exposed to the surface. Tartu, 2022, 130 p.
67. **Tetiana Brodiazhenko**. RelA-SpoT Homolog enzymes as effectors of Toxin-Antitoxin systems. Tartu, 2022, 132 p.
68. **Georg-Marten Lanno**. Development of novel antibacterial drug delivery systems as wound scaffolds using electrospinning technology. Tartu, 2022, 175 p.
69. **Liubov Cherkashchenko**. New insights into alphaviral nsP2 functions. Tartu, 2023, 171 p.
70. **Kristina Kiisholts**. Peptide-based drug carriers and preclinical nanomedicine applications for endometriosis treatment. Tartu, 2023, 138 p.
71. **Kai Rausalu**. Alphaviral nsP2 protease: From requirements for functionality to inhibition. Tartu, 2023, 175 p.
72. **Laura Sandra Lello**. Unraveling the intricate nature of the alphavirus RNA replicase. Tartu, 2023, 219 p.
73. **Houman Masnavi**. Visibility Aware Navigation. Tartu, 2023, 180 p.
74. **Kadir Aktas**. Cosmic Ray Tomography based Object Reconstruction and Recognition. Tartu, 2023, 104 p.
75. **Egils Avots**. Brain abnormality detection using statistical analysis of individual structural connectivity networks and EEG signals. Tartu, 2023, 223 p.
76. **Sainan Wang**. Structure-guided insights into the functions of CHIKV nsP2. Tartu, 2024, 154 p.
77. **Anneli Samel**. Unveiling the characteristics of cancer-testis antigen MAGEA10. Tartu, 2024, 136 p.
78. **Ikechukwu Ofodile**. Fault tolerant attitude control for nanosatellites: ESTCube-2 case. Tartu, 2024, 130 p.
79. **Olena Zamora**. Impacts of plant hormones on controlling stomatal conductance. Tartu, 2024, 166 p.
80. **Mariliis Hinnu**. *In vitro* methods for studying the mechanisms of ribosome-targeting antibiotics. Tartu, 2024, 143 p.
81. **Chung-Yueh Yeh**. Characterization of MPK and HT1 kinases in CO_2-induced stomatal movements. Tartu, 2024, 118 p.
82. **Iman Dadras**. Low power neural network-based control and actuation solutions for insect-scale robots. Tartu, 2024, 149 p.
83. **Fatemeh Rastgar**. Towards reliable real-time trajectory optimization. Tartu, 2024, 158 p.

84. **Maria Maloverjan**. Optimizing cell-penetrating peptide-based nanoparticles for delivery of nucleic acid therapeutics. Tartu, 2024, 172 p.
85. **Joonas Merisalu**. Resistive switching in memristor structures with multilayer dielectrics. Tartu, 2024, 149 p.
86. **Siim Laanesoo**. Novel high-performance biomass-based polymers. Tartu, 2024, 117 p.
87. **Henri Ingelman**. Systems-level characterisation and improvement of *Clostridium autoethanogenum* metabolism. Tartu, 2024, 164 p.
88. **Mailis Laht**. Using the One Health approach for mapping the spread of antibiotic resistant bacteria in Estonia. Tartu, 2024, 188 p.
89. **Ingrid Rebane**. Structure-property relationships of moldable silicone foams. Tartu, 2024, 164 p.
90. **Robert Valner**. Design of TeMoto, a software framework for dependable, adaptive, and collaborative autonomous robots. Tartu, 2024, 182 p.
91. **Kristiina Kurg**. Exploring the potential of a liquid biopsy approach for melanoma diagnostics and the role of extracellular vesicles in atherosclerosis development. Tartu, 2025, 201 p.
92. **Rauno Sedrik**. Synthesis and investigation of polymers from different cyclic bio-based monomers. Tartu, 2025, 155 p.
93. **Alina Ismagilova**. Safety assessment of novel bio-based polymers and compounds used in low carbon technologies. Tartu, 2025, 156 p.
94. **Baiba Brūmele**. Uncovering the TRMT112 methyltransferase network and characterising the cellular functions of TRMT112-network member N6AMT1. Tartu, 2025, 135 p.
95. **Ingmar Tulva**. Causes and consequences of stomatal density in relation to atmospheric humidity. Tartu, 2025, 142 p.
96. **Yauheni Sarokin**. Passive and active liquid mediation in natural and synthetic morphing systems. Tartu, 2025, 173 p.